Photosynth Res (2018) 136:63–82
DOI 10.1007/s11120-017-0439-y

ORIGINAL ARTICLE

Kinetics of photosystem II electron transport: a mathematical analysis based on chlorophyll fluorescence induction

Agu Laisk[1] · **Vello Oja**[1]

Received: 21 April 2017 / Accepted: 28 August 2017 / Published online: 21 September 2017

Abstract The OJDIP rise in chlorophyll fluorescence during induction at different light intensities was mathematically modeled using 24 master equations describing electron transport through photosystem II (PSII) plus ordinary differential equations for electron budgets in plastoquinone, cytochrome *f*, plastocyanin, photosystem I, and ferredoxin. A novel feature of the model is consideration of electron in- and outflow budgets resulting in changes in redox states of Tyrosine Z, P680, and Q_A as sole bases for changes in fluorescence yield during the transient. Ad hoc contributions by transmembrane electric fields, protein conformational changes, or other putative quenching species were unnecessary to account for primary features of the phenomenon, except a peculiar slowdown of intra-PSII electron transport during induction at low light intensities. The lower than F_m post-flash fluorescence yield F_f was related to oxidized tyrosine Z. The transient J peak was associated with equal rates of electron arrival to and departure from Q_A and requires that electron transfer from Q_A^- to Q_B be slower than that from Q_A^- to Q_B^-. Strong quenching by oxidized P680 caused the dip D. Reduced plastoquinone, a competitive product inhibitor of PSII, blocked electron transport proportionally with its concentration. Electron transport rate indicated by fluorescence quenching was faster than the rate indicated by O_2 evolution, because oxidized donor side carriers quench fluorescence but do not transport electrons. The thermal phase of the fluorescence rise beyond the J phase was caused by a progressive increase in the fraction of PSII with reduced Q_A and reduced donor side.

✉ Agu Laisk
alaisk@ut.ee

[1] Institute of Technology, University of Tartu, Nooruse St. 1, Tartu 50411, Estonia

Keywords Photosystem II · Chl fluorescence · Induction · Electron transport · Mathematical model

Abbreviations

F_o	Photochemically quenched fluorescence yield
F_f	Post-flash fluorescence yield
F_m	Maximum unquenched fluorescence yield
FI	Fluorescence induction rise from F_o to F_m
PFD	Photon flux density
TyrZ	Tyrosine Z
STF	Single-turnover flash

Introduction

Chlorophyll fluorescence is an easily measurable signal representing excitations not used for photosynthetic electron transport. A classical understanding is that fluorescence is in its maximum, F_m, when in PSII the photosynthetic electron transfer is blocked by reduction of the first acceptor quinone Q_A (Duysens and Sweers 1963). In many cases, this understanding works well, except when Q_A is reduced very rapidly by single-turnover flashes (STF). During illumination with intensities (PFD) of up to 10,000 μmol m^{-2} s^{-1}, fluorescence begins at the low F_o level and approaches the maximum F_m level after about 300 ms. The slow saturation is explained by fast electron transfer away from Q_A, which stops only after the entire electron transport chain becomes reduced. When PFD is increased to the level of xenon or laser flashes exceeding 1 mol m^{-2} s^{-1}, Q_A becomes reduced faster than oxidized by the electron transfer, so that the F_m-level fluorescence is expected after a few microseconds. In experiments, this does not happen and instead a lower F_f level of fluorescence is recorded at 50 μs after the flash, followed by quenching as Q_A^- is re-oxidized by electron

transfer to Q_B (de Wijn and van Gorkom 2001). A persistent enigma of the "Q_A model" of fluorescence is that the "maximum" fluorescence yield F_f, measured 50 µs after a ST flash, is significantly below the F_m level determined from a second-long multiple-turnover pulse (Joliot and Joliot 1964, 1977, 1981; Neubauer and Schreiber 1987; Samson and Bruce 1996). This has opened possibilities for alternative interpretations, such that the flash-level fluorescence F_f is indeed the actual maximum fluorescence yield, corresponding to blocked charge separation within PSII, but the following "thermal phase" is caused by the release of other, hypothetical quenchers (Delosme 1967; Schreiber and Neubauer 1987; Neubauer and Schreiber 1987). These potential quenchers have been listed (Vredenberg 2008b; Stirbet and Govindjee 2012; Koblížek et al. 2001): (1) $P680^+$ can quench Chl a fluorescence as efficiently as Q_A reduction; (2) P680 triplet, $^3P680$, most likely $^3Chl_{D1}$ quenches in equilibrium with $^3P_{D1}$; (3) carotenoid triplet ^3Car is an efficient quencher in the antenna; (4) non-photochemical quenching by oxidized PQ molecules; (5) reduced $Pheo_{D1}$ may be a quencher due to charge separation equilibrium P680* ↔ $P680^+Pheo^-$, shifted by transmembrane electric field photoelectrochemical quenching (Vredenberg et al. 2009); (6) quenching by charge recombination from Q_B (Schreiber 2002); and (7) quenching by conformational changes in Chl proteins (Schansker et al. 2011).

In this work, we focus on this paradox by mathematical modeling of the fluorescence rise kinetics in terms of gradual reduction of all electron carriers, without a need for excitation quenchers other than photochemical quenching by electron transfer and non-photochemical quenching by oxidized donor side carriers. Models have been created to describe fluorescence induction, differing mainly in mathematical details (Laisk et al. 2009; Lazár and Schansker 2009). A widely applied approach has been to synthesize the complex FI curve with a series of exponentials, each representing a partial reaction approximated by the first-order kinetics (Strasser et al. 2004; Vredenberg 2015). In a more detailed approach, a system of mass action-based ordinary differential equations considered kinetic properties of individual reactions (Baake and Strasser 1990; Baake and Schlöder 1992; Zhu et al. 2005). The most sophisticated approaches apply large systems of first-order master equations to describe transformations among the numerous "forms" of a protein complex, incorporating several redox-related electron carriers (Lazár 2003, 2009, 2013; Lebedeva et al. 2002; Belyaeva et al. 2011, 2015). The model by Lebedeva et al. (2002) involved electron transfer redox reactions, accompanied by the generation of transmembrane field and a proton gradient. The detailed approach by Lazár (2003) involved PSII and the water-splitting complex, covering 12 orders of time magnitude from the excitation of PSII antenna to the reduction of plastoquinone. The model was extended involving Q-cycle and cyclic electron transport, up to a reduction of ferredoxin and $NADP^+$ at the PSI acceptor side (Lazár 2009).

Despite various mathematical techniques, no consensus has yet been established concerning a central question: how are the PSII donor and acceptor side electron transfer processes combined to determine the fluorescence rise from F_o to F_m (Schansker et al. 2011, 2014; Vredenberg 2008b)? There are at least three states (or forms) of the PSII complex co-determining the fluorescence yield: Q_A reduction on the acceptor side and oxidized TyrZ and oxidized P680 on the donor side. In this work, we have designed a mathematical model where these three states, considered together, can determine the whole fluorescence induction with its OJDIP inflections, at least at high light intensities. The experimental observations which were difficult to reconcile with the simple Q_A model (Schansker et al. 2014) can still be reconciled. The principle contradiction—O_2 evolution is much slower than electron transport determined from fluorescence quenching (Laisk and Oja 2013)—is explained by the inability of the donor-oxidized states to transport electrons, though they are still quenching excitation. Competitive rebinding of reduced plastoquinone to the Q_B site on the acceptor side explains the closely proportional dependence of fluorescence on the redox state of this electron carrier.

The model

Applying the mathematical methods used by Lebedeva et al. (2002), Lazár (2003), and Belyaeva et al. (2006, 2011), but grouping PSII internal structure in partial reactions differently from the predecessors, we have constructed a computer model that adequately simulates PSII electron transport and Chl fluorescence in leaves. The model explains the low ST flash-induced fluorescence yield and the OJDIP inflection in the dark-light fluorescence rise on the basis of kinetic restrictions and different quenching properties of electron carriers on the donor and acceptor sides of PSII, without a need to postulate changes in transmembrane electric field, protein conformation, or other potential excitation quenchers. The internal structure of the PSII core is simplified to the sequence YPAB of four electron carriers, where Y is tyrosine Z, P is P680, A is Q_A, and B is Q_B. In this denotation, P680 is the complex of $P_{D1}{\cdot}P_{D2}{\cdot}Chl_{D1}{\cdot}Chl_{D2}{\cdot}Pheo_{D1}{\cdot}Pheo_{D2}$ (Renger 2010). The basic assumption of the model is that the whole coherence complex covering the two PSII branches, but with an exciton mainly concentrating on Chl_{D1}, $P_{D1}{\cdot}P_{D2}$, $Pheo_{D1}$ (Novoderezhkin et al. 2015) and involving the $Pheo_{D1}^-{\cdot}P_{D1}^+$ intermediate charge-separated state, is equilibrated with antenna excitation. The charge-stabilized state with Q_A^- and $P680^+$ is formed as a result of a charge transfer from excited P680* to Q_A via the $Pheo_{D1}^-{\cdot}P_{D1}^+$

intermediate state, but is immediately (within less than 1 µs) reduced by electron transfer to $P680^+$ from TyrZ (Christen et al. 1998), resulting in the $TyrZ_{ox}$·P680 donor complex $Y_oP_rA_rB_{oo}$. Double oxidation of the $TyrZ_{ox}$·P680 pair is rare, but may happen at high PFDs wherein $P680^+$ ($Y_oP_oA_rB_{ro}$ form) accumulates in an appreciable amount.

On the acceptor side, Q_A (denoted A) is the bound quinone primary electron acceptor, from which electrons are transferred to the mobile secondary quinone acceptor Q_B (denoted B). The latter accepts sequentially two electrons, after which reduced plastoquinone (PQH_2) formed in the Q_B site (denoted B_{rr}) equilibrates diffusionally with the free PQH_2 pool. Both quinone forms, PQH_2 and PQ, may leave the Q_B site with a first-order rate constant, but the empty Q_B site may absorb either PQ or PQH_2 competitively, depending on the second-order rate constant and concentration of PQ and PQH_2—as is typical for the active site of an enzyme. Fluorescence transients could be reproduced assuming relatively high affinity of PQH_2 for the Q_B site, which makes this product a strong inhibitor of PSII as the "water–plastoquinone oxidoreductase" enzyme. The fraction of PSII closed due to the doubly reduced Q_B increases in reversible equilibrium about proportionally with the free PQH_2 pool.

A direct output of the model is mechanistic explanation of the kinetic features of the rising fluorescence induction (FI) traces for leaves. For easier comparison with experiment, inputs of the model are incident photon flux density PFD (mol m^{-2} s^{-1}) and Chl content (mol m^{-2}). The area densities of PSII ($PS2_T$) and PSI (PSI_T) are calculated as

$$PS2_T = a_{II} \cdot Chl/PSU_2 \tag{1}$$

and

$$PS1_T = \left(1 - a_{II}\right) \cdot Chl/PSU_1, \tag{2}$$

where a_{II} is partitioning of absorbed excitation to PSII and PSU_2 is the antenna size (Chl per center). Equation 2 is the analogous expression for PSI. Excitation rates per center n_2 and n_1 (s^{-1}) are calculated considering the incident photon flux density (PFD, mol m^{-2} s^{-1}), absorption coefficient (*Labs*), and antenna size:

$$n_2 = PFD \cdot Labs \cdot a_{II}/PS2_T \tag{3}$$

and

$$n_1 = PFD \cdot Labs \cdot \left(1 - a_{II}\right)/PS1_T. \tag{4}$$

The redox states of the YPAB system components or forms (Lazár 2003) are conveniently expressed with subscripts denoting reduction (r) or oxidation (o). For example, after dark adaptation the most likely PSII form is $Y_rP_rA_oB_{oo}$, meaning reduced TyrZ and P680, but oxidized Q_A and Q_B.

Emphasis is placed on the donor side oxidation states, that is the forms containing Y_oP_r and Y_oP_o. After an electron is transferred, the $Y_rP_rA_oB_{oo}$ form becomes $Y_oP_rA_rB_{oo}$. We assume an immediate electron transfer from TyrZ to $P680^+$, precluding the accumulation of Y_rP_o form. The oxidized Y_o receives an electron from an S-state with first-order kinetics, rate constant j_d (for rate constants, the subscript d means "direct" and r means "reverse," but in this analysis we neglect the reversibility of electron donation from TyrZ back to the S-state). The j_d value actually depends on the advancement of the S-state, but for the sake of simplicity we did not include different S-states in the model. Inductions involving the transfer of several electrons are characterized by a single effective j_d value.

The heart of the model is the system of 24 master equations, each describing the budget (derivative, rate of change of the fraction) of the particular YPAB form. The sum of the forms is normalized to 1. In contrast to prior studies, the rate constants of excitation energy capture were normalized to the sum of the physical excitation capture constants (dissipation + triplet formation + fluorescence) = $k_f = 1$. Photosynthetically important rate constants are expressed in relation to the physical constant, e.g., $k_p = 7.5$ (Table 1). As a result, the calculated fluorescence is normalized to $F_m = 1$. The following differential equations describe the transformation of each of the forms, where $d(Y_xP_xA_xB_{xx})/dt$ is the rate of change of the fraction (s^{-1}) of each of these forms.

0 e^- forms:

$$\begin{aligned} d\left(Y_oP_oA_o\right)/dt = {} & -j_d \cdot Y_oP_oA_o + oq_d \cdot Y_oP_oA_oB_{oo} \\ & + rq_d \cdot Y_oP_oA_oB_{rr} - \left(oq_r \cdot PQ + rq_r \cdot PQH_2\right) \cdot Y_oP_oA_o; \end{aligned} \tag{5}$$

$$\begin{aligned} d\left(Y_oP_oA_oB_{oo}\right)/dt = {} & -j_d \cdot Y_oP_oA_oB_{oo} \\ & - oq_d \cdot Y_oP_oA_oB_{oo} + oq_r \cdot PQ \cdot Y_oP_oA_o; \end{aligned} \tag{6}$$

1 e^- forms:

$$\begin{aligned} d\left(Y_oP_rA_o\right)/dt = {} & j_d \cdot Y_oP_oA_o - j_d \cdot Y_oP_rA_o + rq_d \cdot Y_oP_rA_oB_{rr} \\ & + oq_d \cdot Y_oP_rA_oB_{oo} - \left(oq_r \cdot PQ + rq_r \cdot PQH_2\right) \cdot Y_oP_rA_o \\ & - n_2 \cdot k_p/\left(1 + k_p + k_n + k_r\right) \cdot Y_oP_rA_o; \end{aligned} \tag{7}$$

$$\begin{aligned} d\left(Y_oP_oA_r\right)/dt = {} & -j_d \cdot Y_oP_oA_r \\ & + n_2 \cdot k_p/\left(1 + k_p + k_n + k_r\right) \cdot Y_oP_rA_o \\ & + rq_d \cdot Y_oP_oA_rB_{rr} + oq_d \cdot Y_oP_oA_rB_{oo} \\ & - \left(oq_r \cdot PQ + rq_r \cdot PQH_2\right) \cdot Y_oP_oA_r; \end{aligned} \tag{8}$$

$$\begin{aligned} d\left(Y_oP_rA_oB_{oo}\right)/dt = {} & -j_d \cdot Y_oP_rA_oB_{oo} + j_d \cdot Y_oP_oA_oB_{oo} \\ & - n_2 \cdot k_p/\left(1 + k_p + k_n + k_r\right) \cdot Y_oP_rA_oB_{oo} \\ & - oq_d \cdot Y_oP_rA_oB_{oo} + oq_r \cdot PQ \cdot Y_oP_rA_o; \end{aligned} \tag{9}$$

$$\begin{aligned} d\left(Y_oP_oA_rB_{oo}\right)/dt = {} & -j_d \cdot Y_oP_oA_rB_{oo} \\ & + n_2 \cdot k_p/\left(1 + k_p + k_n + k_r\right) \cdot Y_oP_rA_oB_{oo} \\ & + oq_r \cdot PQ \cdot Y_oP_oA_r - oq_d \cdot Y_oP_oA_rB_{oo} \\ & - b1_d \cdot Y_oP_oA_rB_{oo} + b1_r \cdot Y_oP_oA_oB_{ro}; \end{aligned} \tag{10}$$

Table 1 Parameter values

PFD	3E−3	mol m^{-2} s^{-1} (variable)
Labs	0.86	Light absorption coefficient
Chl	3E−4	mol m^{-2}
a_{II}	0.5	Excitation partitioning to PSII
PSU2	170	Chl per PSII
PSU1	170	Chl per PSI
PQ_T	5	Plastoquinone per PSII
$Cytf_T$	1	Cytochrome *f* per PSII
PC_T	2	Plastocyanin per PSII
FD_T	5	Ferredoxin per PSII
k_n	0	Non-photochemical quenching
k_r	0.5	Quenching by $TyrZ_{ox}$
k_p	7.5	Photochemical quenching
k_f	1.0	Fluorescence emission = 1, other constants relative to k_f
j_d	2000	e^- donation from an S-state, s^{-1}
$b1_d$	2000	$Q_A \rightarrow Q_B$, first electron, s^{-1}
kE_1	20	$Q_A \leftrightarrow Q_B$ equilibrium constant for the first electron
$b2_d$	5000	$Q_A \rightarrow Q_B$, second electron, s^{-1}
oq_d	1000	Dissociation of PQ from Q_B, s^{-1}
oq_r	2000	Re-association of PQ with Q_B, s^{-1} per PQ
rq_d	2000	Dissociation of PQH_2 from Q_B, s^{-1}
rq_r	5000	Re-association of PQH_2 with Q_B, s^{-1} per PQH_2
k_{b6f}	50	PQH_2 oxidation by Cyt b_6f, s^{-1}
kE_{b6f}	1000	Equilibrium constant $PQH_2 \leftrightarrow$ Cytf
k_{cytf}	1000	Cytf oxidation, s^{-1}
kE_{cytf}	3.0	Equilibrium constant Cytf $\leftrightarrow$ PC
k_{pc}	1000	PC oxidation, s^{-1}
kE_{pc}	35	Equilibrium constant PC $\leftrightarrow$ P700
k_{fx}	1000	FX oxidation, s^{-1}
kE_{fx}	100	Equilibrium constant FX $\leftrightarrow$ FD
k_{fd}	0.0	FD oxidation, s^{-1}

$$\begin{aligned}\mathrm{d}\left(\mathrm{Y_oP_oA_oB_{ro}}\right)/\mathrm{d}t = {} & -j_\mathrm{d}\cdot\mathrm{Y_oP_oA_oB_{ro}} \\ & + b1_\mathrm{d}\cdot\mathrm{Y_oP_oA_rB_{oo}} - b1_\mathrm{r}\cdot\mathrm{Y_oP_oA_oB_{ro}};\end{aligned} \tag{11}$$

2 e^- forms:

$$\begin{aligned}\mathrm{d}\left(\mathrm{Y_rP_rA_o}\right)/\mathrm{d}t = {} & j_\mathrm{d}\cdot\mathrm{Y_oP_rA_o} \\ & - n_2\cdot k_\mathrm{p}/\left(1+k_\mathrm{p}+k_\mathrm{n}\right)\cdot\mathrm{Y_rP_rA_o} \\ & + rq_\mathrm{d}\cdot\mathrm{Y_rP_rA_oB_{rr}} + oq_\mathrm{d}\cdot\mathrm{Y_rP_rA_oB_{oo}} \\ & - \left(oq_\mathrm{r}\cdot\mathrm{PQ} + rq_\mathrm{r}\cdot\mathrm{PQH_2}\right)\cdot\mathrm{Y_rP_rA_o};\end{aligned} \tag{12}$$

$$\begin{aligned}\mathrm{d}\left(\mathrm{Y_oP_rA_r}\right)/\mathrm{d}t = {} & j_\mathrm{d}\cdot\mathrm{Y_oP_oA_r} - j_\mathrm{d}\cdot\mathrm{Y_oP_rA_r} \\ & + n_2\cdot k_\mathrm{p}/\left(1+k_\mathrm{p}+k_\mathrm{n}\right)\cdot\mathrm{Y_rP_rA_o} \\ & + rq_\mathrm{d}\cdot\mathrm{Y_oP_rA_rB_{rr}} + oq_\mathrm{d}\cdot\mathrm{Y_oP_rA_rB_{oo}} \\ & - \left(oq_\mathrm{r}\cdot\mathrm{PQ} + rq_\mathrm{r}\cdot\mathrm{PQH_2}\right)\cdot\mathrm{Y_oP_rA_r};\end{aligned} \tag{13}$$

$$\begin{aligned}\mathrm{d}\left(\mathrm{Y_rP_rA_oB_{oo}}\right)/\mathrm{d}t = {} & j_\mathrm{d}\cdot\mathrm{Y_oP_rA_oB_{oo}} \\ & - n_2\cdot k_\mathrm{p}/\left(1+k_\mathrm{p}+k_\mathrm{n}\right)\cdot\mathrm{Y_rP_rA_oB_{oo}} \\ & + oq_\mathrm{r}\cdot\mathrm{PQ}\cdot\mathrm{Y_rP_rA_o} - oq_\mathrm{d}\cdot\mathrm{Y_rP_rA_oB_{oo}};\end{aligned} \tag{14}$$

$$\begin{aligned}\mathrm{d}\left(\mathrm{Y_oP_rA_rB_{oo}}\right)/\mathrm{d}t = {} & j_\mathrm{d}\cdot\mathrm{Y_oP_oA_rB_{oo}} - j_\mathrm{d}\cdot\mathrm{Y_oP_rA_rB_{oo}} \\ & + n_2\cdot k_\mathrm{p}/\left(1+k_\mathrm{p}+k_\mathrm{n}\right)\cdot\mathrm{Y_rP_rA_oB_{oo}} - b1_\mathrm{d}\cdot\mathrm{Y_oP_rA_rB_{oo}} \\ & + b1_\mathrm{r}\cdot\mathrm{Y_oP_rA_oB_{ro}} - oq_\mathrm{d}\cdot\mathrm{Y_oP_rA_rB_{oo}} + oq_\mathrm{r}\cdot\mathrm{PQ}\cdot\mathrm{Y_oP_rA_r};\end{aligned} \tag{15}$$

$$\begin{aligned}\mathrm{d}\left(\mathrm{Y_oP_rA_oB_{ro}}\right)/\mathrm{d}t = {} & j_\mathrm{d}\cdot\mathrm{Y_oP_oA_oB_{ro}} - j_\mathrm{d}\cdot\mathrm{Y_oP_rA_oB_{ro}} \\ & - n_2\cdot k_\mathrm{p}/\left(1+k_\mathrm{p}+k_\mathrm{n}+k_\mathrm{r}\right)\cdot\mathrm{Y_oP_rA_oB_{ro}} \\ & + b1_\mathrm{d}\cdot\mathrm{Y_oP_rA_rB_{oo}} - b1_\mathrm{r}\cdot\mathrm{Y_oP_rA_oB_{ro}};\end{aligned} \tag{16}$$

$$\begin{aligned}\mathrm{d}\left(\mathrm{Y_oP_oA_rB_{ro}}\right)/\mathrm{d}t = {} & -j_\mathrm{d}\cdot\mathrm{Y_oP_oA_rB_{ro}} \\ & + n_2\cdot k_\mathrm{p}/\left(1+k_\mathrm{p}+k_\mathrm{n}+k_\mathrm{r}\right)\cdot\mathrm{Y_oP_rA_oB_{ro}} \\ & - b2_\mathrm{d}\cdot\mathrm{Y_oP_oA_rB_{ro}};\end{aligned} \tag{17}$$

$$\begin{aligned}\mathrm{d}\left(\mathrm{Y_oP_oA_oB_{rr}}\right)/\mathrm{d}t = {} & -j_\mathrm{d}\cdot\mathrm{Y_oP_oA_oB_{rr}}\\ & + b2_\mathrm{d}\cdot\mathrm{Y_oP_oA_rB_{ro}} + rq_\mathrm{r}\cdot\mathrm{PQH_2}\cdot\mathrm{Y_oP_oA_o}\\ & - rq_\mathrm{d}\cdot\mathrm{Y_oP_oA_oB_{rr}};\end{aligned} \tag{18}$$

3 e^- forms:

$$\begin{aligned}\mathrm{d}\left(\mathrm{Y_rP_rA_r}\right)/\mathrm{d}t = {} & j_\mathrm{d}\cdot\mathrm{Y_oP_rA_r} + rq_\mathrm{d}\cdot\mathrm{Y_rP_rA_rB_{rr}}\\ & + oq_\mathrm{d}\cdot\mathrm{Y_rP_rA_rB_{oo}} - (oq_\mathrm{r}\cdot\mathrm{PQ} + rq_\mathrm{r}\cdot\mathrm{PQH_2})\cdot\mathrm{Y_rP_rA_r};\end{aligned} \tag{19}$$

$$\begin{aligned}\mathrm{d}\left(\mathrm{Y_rP_rA_rB_{oo}}\right)/\mathrm{d}t = {} & j_\mathrm{d}\cdot\mathrm{Y_oP_rA_rB_{oo}} - b1_\mathrm{d}\cdot\mathrm{Y_rP_rA_rB_{oo}}\\ & + b1_r\cdot\mathrm{Y_rP_rA_oB_{ro}} + oq_\mathrm{r}\cdot\mathrm{PQ}\cdot\mathrm{Y_rP_rA_r} - oq_\mathrm{d}\cdot\mathrm{Y_rP_rA_rB_{oo}};\end{aligned} \tag{20}$$

$$\begin{aligned}\mathrm{d}\left(\mathrm{Y_oP_rA_rB_{ro}}\right)/\mathrm{d}t = {} & j_\mathrm{d}\cdot\mathrm{Y_oP_oA_rB_{ro}} - j_\mathrm{d}\cdot\mathrm{Y_oP_rA_rB_{ro}}\\ & + n_2\cdot k_\mathrm{p}/\left(1 + k_\mathrm{p} + k_\mathrm{n}\right)\cdot\mathrm{Y_rP_rA_oB_{ro}} - b2_\mathrm{d}\cdot\mathrm{Y_oP_rA_rB_{ro}};\end{aligned} \tag{21}$$

$$\begin{aligned}\mathrm{d}\left(\mathrm{Y_oP_rA_oB_{rr}}\right)/\mathrm{d}t = {} & j_\mathrm{d}\cdot\mathrm{Y_oP_oA_oB_{rr}} - j_\mathrm{d}\cdot\mathrm{Y_oP_rA_oB_{rr}}\\ & - n_2\cdot k_\mathrm{p}/\left(1 + k_\mathrm{p} + k_\mathrm{n} + k_\mathrm{r}\right)\cdot\mathrm{Y_oP_rA_oB_{rr}}\\ & + b2_\mathrm{d}\cdot\mathrm{Y_oP_rA_rB_{ro}} - rq_\mathrm{d}\cdot\mathrm{Y_oP_rA_oB_{rr}}\\ & + rq_\mathrm{r}\cdot\mathrm{PQH_2}\cdot\mathrm{Y_oP_rA_o};\end{aligned} \tag{22}$$

$$\begin{aligned}\mathrm{d}\left(\mathrm{Y_rP_rA_oB_{ro}}\right)/\mathrm{d}t = {} & j_\mathrm{d}\cdot\mathrm{Y_oP_rA_oB_{ro}}\\ & - n_2\cdot k_\mathrm{p}/\left(1 + k_\mathrm{p} + k_\mathrm{n}\right)\cdot\mathrm{Y_rP_rA_oB_{ro}}\\ & + b1_\mathrm{d}\cdot\mathrm{Y_rP_rA_rB_{oo}} - b1_\mathrm{r}\cdot\mathrm{Y_rP_rA_oB_{ro}};\end{aligned} \tag{23}$$

$$\begin{aligned}\mathrm{d}\left(\mathrm{Y_oP_oA_rB_{rr}}\right)/\mathrm{d}t = {} & -j_\mathrm{d}\cdot\mathrm{Y_oP_oA_rB_{rr}}\\ & + n_2\cdot k_\mathrm{p}/(1 + k_\mathrm{p} + k_\mathrm{n} + k_\mathrm{r})\cdot\mathrm{Y_oP_rA_oB_{rr}}\\ & - rq_\mathrm{d}\cdot\mathrm{Y_oP_oA_rB_{rr}} + rq_\mathrm{r}\cdot\mathrm{PQH_2}\cdot\mathrm{Y_oP_oA_r};\end{aligned} \tag{24}$$

4 e^- forms:

$$\mathrm{d}\left(\mathrm{Y_rP_rA_rB_{ro}}\right)/\mathrm{d}t = j_\mathrm{d}\cdot\mathrm{Y_oP_rA_rB_{ro}} - b2_\mathrm{d}\cdot\mathrm{Y_rP_rA_rB_{ro}}; \tag{25}$$

$$\begin{aligned}\mathrm{d}\left(\mathrm{Y_rP_rA_oB_{rr}}\right)/\mathrm{d}t = {} & j_\mathrm{d}\cdot\mathrm{Y_oP_rA_oB_{rr}}\\ & - n_2\cdot k_\mathrm{p}/\left(1 + k_\mathrm{p} + k_\mathrm{n}\right)\cdot\mathrm{Y_rP_rA_oB_{rr}}\\ & + b2_\mathrm{d}\cdot\mathrm{Y_rP_rA_rB_{ro}} - rq_\mathrm{d}\cdot\mathrm{Y_rP_rA_oB_{rr}}\\ & + rq_\mathrm{r}\cdot\mathrm{PQH_2}\cdot\mathrm{Y_rP_rA_o};\end{aligned} \tag{26}$$

$$\begin{aligned}\mathrm{d}\left(\mathrm{Y_oP_rA_rB_{rr}}\right)/\mathrm{d}t = {} & j_\mathrm{d}\cdot\mathrm{Y_oP_oA_rB_{rr}} - j_\mathrm{d}\cdot\mathrm{Y_oP_rA_rB_{rr}}\\ & + n_2\cdot k_\mathrm{p}/\left(1 + k_\mathrm{p} + k_\mathrm{n}\right)\cdot\mathrm{Y_rP_rA_oB_{rr}}\\ & - rq_\mathrm{d}\cdot\mathrm{Y_oP_rA_rB_{rr}} + rq_\mathrm{r}\cdot\mathrm{PQH_2}\cdot\mathrm{Y_oP_rA_r};\end{aligned} \tag{27}$$

5 e^- forms:

$$\begin{aligned}\mathrm{d}\left(\mathrm{Y_rP_rA_rB_{rr}}\right)/\mathrm{d}t = {} & j_\mathrm{d}\cdot\mathrm{Y_oP_rA_rB_{rr}} - rq_\mathrm{d}\cdot\mathrm{Y_rP_rA_rB_{rr}}\\ & + rq_\mathrm{r}\cdot\mathrm{PQH_2}\cdot\mathrm{Y_rP_rA_r}.\end{aligned} \tag{28}$$

Equations (5–28) contain forms $\mathrm{Y_xP_xA_xB_{rr}}$ and $\mathrm{Y_xP_xA_xB_{oo}}$ with doubly reduced and doubly oxidized $\mathrm{Q_B}$, which reversibly dissociates, joining the diffusible $\mathrm{PQH_2}$ and PQ pools, whose level is determined by the following budget equations:

$$\begin{aligned}\mathrm{dPQH_2}/\mathrm{d}t = {} & rq_\mathrm{d}\cdot\left(\mathrm{Y_oP_oA_oB_{rr}} + \mathrm{Y_oP_rA_oB_{rr}} + \mathrm{Y_oP_oA_rB_{rr}}\right.\\ & \left.+\mathrm{Y_rP_rA_oB_{rr}} + \mathrm{Y_oP_rA_rB_{rr}} + \mathrm{Y_rP_rA_rB_{rr}}\right)\\ & - rq_\mathrm{r}\cdot\mathrm{PQH_2}\cdot\left(\mathrm{Y_oP_oA_o} + \mathrm{Y_oP_rA_o} + \mathrm{Y_oP_oA_r}\right.\\ & \left.+\mathrm{Y_rP_rA_o} + \mathrm{Y_oP_rA_r} + \mathrm{Y_rP_rA_r}\right) - V_\mathrm{b6f},\end{aligned} \tag{29}$$

$$\begin{aligned}\mathrm{dPQ}/\mathrm{d}t = {} & oq_\mathrm{d}\cdot\left(\mathrm{Y_oP_oA_oB_{oo}} + \mathrm{Y_oP_rA_oB_{oo}} + \mathrm{Y_oP_oA_rB_{oo}}\right.\\ & \left.+\mathrm{Y_rP_rA_oB_{oo}} + \mathrm{Y_oP_rA_rB_{oo}} + \mathrm{Y_rP_rA_rB_{oo}}\right)\\ & - oq_\mathrm{r}\cdot\mathrm{PQ}\cdot\left(\mathrm{Y_oP_oA_o} + \mathrm{Y_oP_rA_o} + \mathrm{Y_oP_oA_r}\right.\\ & \left.+\mathrm{Y_rP_rA_o} + \mathrm{Y_oP_rA_r} + \mathrm{Y_rP_rA_r}\right) + V_\mathrm{b6f},\end{aligned} \tag{30}$$

$$\text{where } \mathrm{V_{b6f}} := k_\mathrm{b6f}\cdot\left(\mathrm{PQH_2}\cdot\mathrm{Cytf_o} - \mathrm{Cytf_r}\cdot\mathrm{PQ}/kE_\mathrm{b6f}\right). \tag{31}$$

Equation (31) describes electron transport through the Q-cycle in the Cyt $\mathrm{b_6f}$ complex. Although the Q-cycle is a complex reaction system (Lebedeva et al. 2002), its overall kinetics are well represented by two first-order reactions in series (Laisk et al. 2016). Here we neglect the two-step nature of the process, but apply single first-order reaction kinetics with respect to $\mathrm{PQH_2}$. Although being first-order, with increasing $\mathrm{PQH_2}$ level the reaction rate still becomes limited by the availability of oxidized Cyt *f* as an electron acceptor.

Electron transfer between Cyt *f*, PC, and P700 is very fast, being close to redox equilibrium (Oja et al. 2010). In the Cyt $\mathrm{b_6f}$ complex, the Q-cycle reduces 2 Cyt *f* at the expense of oxidation of one $\mathrm{PQH_2}$. From $\mathrm{Cytf_r}$ electrons rapidly leave, reducing oxidized PC with the first-order kinetics:

$$\mathrm{dCytf_r}/\mathrm{d}t = 2\cdot V_\mathrm{b6f} - k_\mathrm{cytf}\cdot\left(\mathrm{Cytf_r}\cdot\mathrm{PC_o} - \mathrm{Cytf_o}\cdot\mathrm{PC_r}/kE_\mathrm{cytf}\right). \tag{32}$$

Plastocyanin is oxidized by electron transfer to $\mathrm{P700^+}$:

$$\begin{aligned}\mathrm{dPC_r}/\mathrm{d}t = {} & k_\mathrm{cytf}\cdot\left(\mathrm{Cytf_r}\cdot\mathrm{PC_o} - \mathrm{Cytf_o}\cdot\mathrm{PC_r}/kE_\mathrm{cytf}\right)\\ & - k_\mathrm{PC}\cdot\left(\mathrm{PC_r}\cdot\mathrm{P700_o} - \mathrm{PC_o}\cdot\mathrm{P700_r}/kE_\mathrm{pc}\right),\end{aligned} \tag{33}$$

$$\begin{aligned}\mathrm{dP700_r}/\mathrm{d}t = {} & k_\mathrm{PC}\cdot\left(\mathrm{PC_r}\cdot\mathrm{P700_o} - \mathrm{PC_o}\cdot\mathrm{P700_r}/kE_\mathrm{pc}\right)\\ & - n_1\cdot\mathrm{P700_r}\cdot\mathrm{FX_o},\end{aligned} \tag{34}$$

$$\mathrm{dFX_r}/\mathrm{d}t = n_1\cdot\mathrm{P700_r}\cdot\mathrm{FX_o} - k_\mathrm{fx}\cdot\left(\mathrm{FX_r}\cdot\mathrm{FD_o} - \mathrm{FX_o}\cdot\mathrm{FD_r}/kE_\mathrm{fx}\right), \tag{35}$$

$$\mathrm{dFD_r}/\mathrm{d}t = k_\mathrm{fx}\cdot\left(\mathrm{FX_r}\cdot\mathrm{FD_o} - \mathrm{FX_o}\cdot\mathrm{FD_r}/kE_\mathrm{fx}\right) - k_\mathrm{fd}\cdot\mathrm{FD_r}. \tag{36}$$

In the latter equations (31–36), the oxidized form is found as the difference (total pool − reduced form). In Eqs. (34, 35),

n_1 is the PSI excitation rate (Eq. 4) and only those PSI are photochemically 100% efficient whose P700 is reduced and the primary acceptor (denoted FX) is oxidized. Equilibrium constants kE were adjusted to $kE_{cytf} = 3$, $kE_{pc} = 35$, and $kE_{fx} = 100$ (Oja et al. 2010; Laisk et al. 2016). The large equilibrium constants kE_{cytf} and kE_{pc} ensure free electron flow through the Cyt b_6f complex, while electrons accumulate on the PSI donor side and the large kE_{fx} avoids the blockade on the acceptor side. As PSII room-temperature Chl fluorescence is only indirectly influenced by PSI electron transport via the redox sequence of electron carriers, we used ordinary differential equations for this part of the electron transport chain.

The amount of electrons transported through PSII donor side, measurable as $4{\cdot}O_2$ evolution, e^- per PSII, is expressed as follows:

$$\begin{aligned} \mathrm{dSumO_2}/\mathrm{d}t = \; & j_\mathrm{d} \cdot (\mathrm{Y_oP_oA_o} + \mathrm{Y_oP_oA_oB_{oo}} + \mathrm{Y_oP_rA_o} \\ & + \mathrm{Y_oP_oA_r} + \mathrm{Y_oP_rA_oB_{oo}} + \mathrm{Y_oP_oA_rB_{oo}} + \mathrm{Y_oP_oA_oB_{ro}} \\ & + \mathrm{Y_oP_rA_r} + \mathrm{Y_oP_rA_rB_{oo}} + \mathrm{Y_oP_rA_oB_{ro}} + \mathrm{Y_oP_oA_rB_{ro}} \\ & + \mathrm{Y_oP_oA_oB_{rr}} + \mathrm{Y_oP_rA_rB_{ro}} + \mathrm{Y_oP_rA_oB_{rr}} + \mathrm{Y_oP_oA_rB_{rr}} \\ & + \mathrm{Y_oP_rA_rB_{rr}}). \end{aligned} \tag{37}$$

Equation (37) actually presents the electron transport rate, so for better comparison with experiments based on light pulsing an integrated amount of electrons is calculated for each time moment.

Different Chl fluorescence yield was ascribed to each distinct PSII form. The forms with reduced donor and primary acceptor, $\mathrm{Y_rP_rA_rB_{xx}}$ (independent of whether xx is oo, ro, or rr), emit fluorescence at the maximum yield F_m, normalized to unity in the absence of non-photochemical quenching. The forms with reduced donor and oxidized primary acceptor, $\mathrm{Y_rP_rA_oB_{xx}}$, emit at the F_o yield. Forms with oxidized TyrZ, but reduced P680, $\mathrm{Y_oP_rA_rB_{xx}}$, are assumed to emit at an intermediate "flash" level F_f, which is about a half to two-thirds of the F_m value, dependent on the constant $k_r = 1$ or 0.5. In units with Y_o and A_o, fluorescence is below F_o, rather close to zero ($k_q > 2\,k_p$) (Steffen et al. 2005). Thus, the PSII fluorescence is calculated as follows:

$$\begin{aligned} Fl := \; & 1/\left(1 + k_n + k_r + k_q\right) \cdot (\mathrm{Y_oP_oA_o} + \mathrm{Y_oP_oA_oB_{oo}} \\ & + \mathrm{Y_oP_oA_oB_{ro}} + \mathrm{Y_oP_oA_oB_{rr}} + \mathrm{Y_oP_oA_r} \\ & + \mathrm{Y_oP_oA_rB_{oo}} + \mathrm{Y_oP_oA_rB_{ro}} + \mathrm{Y_oP_oA_rB_{rr}}) \\ & + 1/\left(1 + k_\mathrm{p} + k_\mathrm{n} + k_\mathrm{r}\right) \cdot \left(\mathrm{Y_oP_rA_o}\right. \\ & \left.+\mathrm{Y_oP_rA_oB_{oo}} + \mathrm{Y_oP_rA_oB_{ro}} + \mathrm{Y_oP_rA_oB_{rr}}\right) \\ & + 1/\left(1 + k_\mathrm{n} + k_\mathrm{r}\right) \cdot \left(\mathrm{Y_oP_rA_r} + \mathrm{Y_oP_rA_rB_{oo}}\right. \\ & \left.+\mathrm{Y_oP_rA_rB_{ro}} + \mathrm{Y_oP_rA_rB_{rr}}\right) \\ & + 1/\left(1 + k_\mathrm{p} + k_\mathrm{n}\right) \cdot \left(\mathrm{Y_rP_rA_o} + \mathrm{Y_rP_rA_oB_{oo}}\right. \\ & \left.+\mathrm{Y_rP_rA_oB_{ro}} + \mathrm{Y_rP_rA_oB_{rr}}\right) + 1/\left(1 + k_\mathrm{n}\right) \cdot \left(\mathrm{Y_rP_rA_r}\right. \\ & \left.+\mathrm{Y_rP_rA_rB_{oo}} + \mathrm{Y_rP_rA_rB_{ro}} + \mathrm{Y_rP_rA_rB_{rr}}\right), \end{aligned} \tag{38}$$

where the last term represents forms emitting at F_m, but the yield decreases progressively in the preceding terms. In principle, Eq. (38) states that "closed" centers emit fluorescence (Duysens and Sweers 1963), but differently dependent on the reduction state of their donor and acceptor side carriers. In the calculations, the rate constant for non-photochemical quenching $k_n = 0$, i.e., F_m, is at its maximum "predawn" value and normalized to unity. For comparison with O_2 evolution, electron transport was calculated from fluorescence as

$$\mathrm{dSumF}/\mathrm{d}t = n_2 \cdot (1 - Fl). \tag{39}$$

Equation (39) also presents the electron transport rate, as does Eq. (37), but the sum of transferred electrons per PSII is calculated for each time moment during an induction.

Reduced ferredoxin FD_r is the end of the dark-adapted electron transport sequence. Although the absolute PSII density $PS2_T$ was calculated for every preset Chl content and antenna size, for calculations the sum of all PSII partial states was normalized to unity. For convenience, pool sizes of electron carriers were expressed in relation to PSII density, e.g., $PQ_T = 5$, but antenna sizes and Chl partitioning were chosen such that $PSII_T = PSI_T$.

These equations were solved by computer using the parameters shown in Table 1, modified as shown in the figure legends when necessary. Euler's method was used by automatically adjusting the time step dt so as not to exceed a change of 0.1% of the amplitude of the fastest changing variable. This stabilized the system even during very steep changes in the rate (e.g., ST flash light of 10 mol photons $m^{-2}\ s^{-1}$).

Results

The model was tuned on the basis of experimental FI curves presented in Figs. 1 and 3 of Schansker et al. (2011). Although the Chl content of leaves typically approaches 400–600 µmol m^{-2}, in calculations Chl was set at 300 µmol m^{-2}. Such a choice was an attempt to minimize distortions arising from the gradient in photon density in the leaf cross-section during measurements: most of the photons are absorbed in the upper leaf layer, and most of the fluorescence is detected from the upper layer, accommodating only a part of the whole leaf chlorophyll (Sušila et al. 2004). Partitioning of Chl to PSII was set at $a_{II} = 0.5$, and antenna sizes were chosen $PSU_2 = PSU_1 = 170$ Chl. This resulted in equal PSII and PSI densities $PS2_T = PS1_T = 0.88$ µmol m^{-2}, actively participating in the modeled process. With these parameters, PSI electron transport slightly exceeded that of PSII—due to the losses in PSII caused by fluorescence emission—resulting in about 10% oxidation of P700 during steady-state exposure to a low PFD of 30 µmol $m^{-2}\ s^{-1}$.

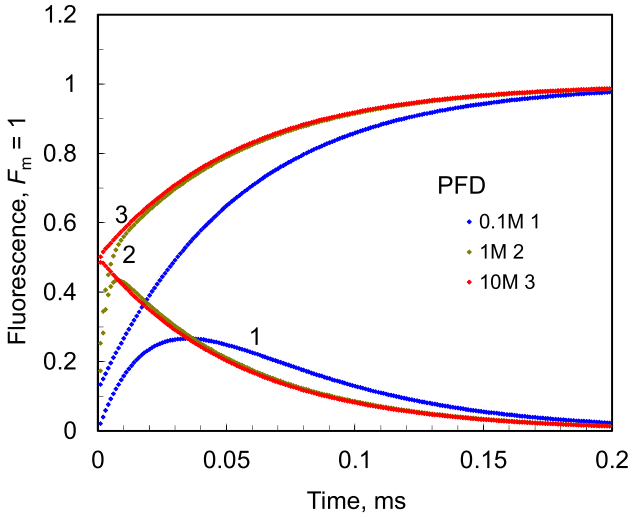

Fig. 1 Simulating a DCMU-poisoned leaf. A very high light (PFD as shown in the panel, mol m^{-2} s^{-1}) was turned on at Time = 0. Upper line shows the time course of total fluorescence, and lower line of the same color shows fluorescence emitted by the donor-oxidized form $Y_oP_rA_r(B_{rr})$. Electron transfer from Q_A to Q_B was blocked by setting $b1_d = b2_d = 0$ (equivalent to the B_{rr} state). Electron donation rate j_d = 18,200 s^{-1}, characteristic of the S_1 state

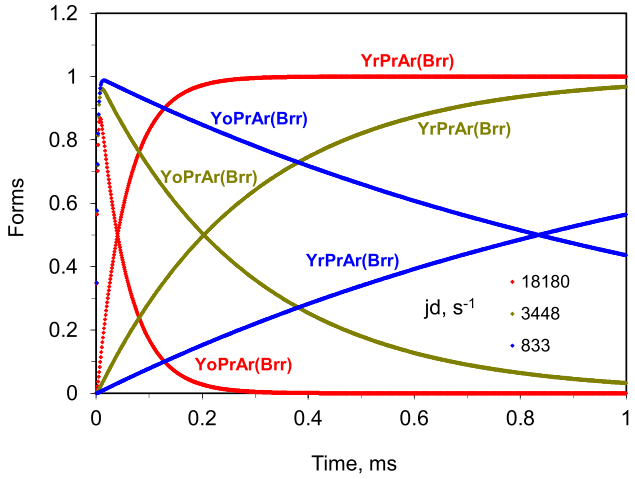

Fig. 2 Dependence on the S-state. Electron donation rate, j_d, was varied in accordance with the dominating S-state number: 18,180 s^{-1} (S_1 to S_2 red), 3448 s^{-1} (S_2 to S_3 green), and 833 s^{-1} (S_3 to S_4 to S_0 blue). At PFD of 1 mol m^{-2} s^{-1}, the upper line shows the time course of accumulation of the $Y_rA_r(B_{rr})$ form, and lower line of the same color shows re-reduction of the $Y_oP_rA_r(B_{rr})$ form

The DCMU case

Responses of the model were systematically investigated from simpler to more complex situations, adjusting the parameters towards better fit to the experimental examples, mainly as reported in Schansker et al. (2011). Best-fit coincidence of the calculated and measured traces was not attempted, rather qualitative reproduction of characteristic features—such as timing and shape of the JIP inflections—was the objective.

The DCMU-inhibited case was modeled by blocking the electron flow between A_r and B_{oo} (Q_A and Q_B) by setting the rate constants $b1_d$ (for the first electron) and $b2_d$ (for the second electron transfer) to zero. The initial state $Y_rP_rA_o(B_{rr})$ is converted to the state $Y_oP_rA_r(B_{rr})$ upon the onset of light (electron transfer from Y_r to P_o is immediate), which is re-reduced to $Y_rP_rA_r(B_{rr})$ by transfer from an S-state. A very high xenon flash illumination of 10 mol m^{-2} s^{-1} was necessary to accomplish electron transfer in all PSII centers within 5 µs (an approximate Xe flash length, Fig. 1). Toward the end of the flash fluorescence yield becomes equal to $F_f = 0.5\ F_m$, as defined by the rate constant $k_r = 1$, competing for excitation quenching in the $Y_oP_rA_r(B_{rr})$ form (parentheses indicate that the Q_B site is occupied by DCMU). This low yield rapidly increases thanks to fast electron donation from the S_1 state (j_d = 18,200 s^{-1}). After 50 µs, the yield is already 0.8 F_m, approaching F_m beyond 100 µs (normalized $F_m = 1$, corresponding to Q_A and donor side carriers reduced in all PSII). The fast electron donation from the S_1 state makes it difficult to measure the time course of fluorescence approaching F_m in the presence of DCMU. Flash power is also critical—1 M (million µmol m^{-2} s^{-1}) is still a sufficient intensity, but with 0.1 M the characteristic fluorescence yield at 50 µs past the flash is significantly unsaturated.

Electron transfer time from an S-state to TyrZ depends on the number of the S-states, being 250 µs from S_0 to S_1, 55 µs from S_1 to S_2, 290 µs from S_2 to S_3, and 1200 µs from S_3 to S_0 (Rappaport et al. 1994). Fluorescence traces of Fig. 1 were calculated with the fast rate constant of the $S_1 \rightarrow S_2$ transfer (j_d = 18,180 s^{-1}), dominating in the dark-adapted state. Slower electron donation from other S-states causes slower substitution of the flash-generated $Y_oP_rA_r(B_{rr})$ form with $Y_rP_rA_r(B_{rr})$: $S_2 \rightarrow S_3$ (j_d = 3448) and $S_3 \rightarrow S_4 \rightarrow S_0$ (j_d = 833 s^{-1}, Fig. 2).

In longer transients below, where more than one electron is transferred, we applied some effective averaged j_d values. Extremely low j_d values of 200 and 20 s^{-1} (Fig. 3) closely reproduced the DCMU-inhibited fluorescence inductions recorded at the negative temperatures of −20 °C and lower (Fig. 3 in Schansker et al. 2011).

$Q_A \rightarrow Q_B$ electron transfer

In this section, the two electrons accumulate at Q_B, but electron transfer from Q_B to PQ is blocked by zeroing the rate constants for dissociation from and association with the Q_B site of the reduced and oxidized plastoquinone species: $rq_d = oq_d = rq_r = oq_r = 0$. The initial condition (dominating form) was set $Y_rP_rA_oB_{oo} = 1$ (PSII donor side reduced, acceptor

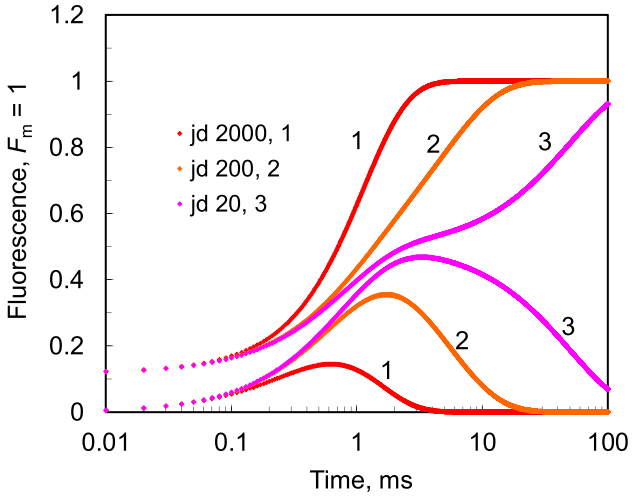

Fig. 3 Extremely slow electron donation. Electron donation rate j_d was slowed down in a DCMU-poisoned leaf in order to simulate the low-temperature measurements of Fig. 3 in Schansker et al. (2011). PFD = 3000 µmol m^{-2} s^{-1}. *Upper line* shows total fluorescence, and *lower line* of the *same color* shows fluorescence emitted by the $Y_oP_rA_r(B_{rr})$ form

side oxidized) and three additional electrons were accumulated until the form $Y_rP_rA_rB_{rr}$ approached unity.

At the high PFD of 15,000 µmol m^{-2} s^{-1}, the modeled fluorescence approaches F_m at about 3 ms. The characteristic J inflection is present in this transient, though donor side limitation was set absent (Fig. 4a). Importantly, the J inflection is present when the first $Q_A \rightarrow Q_B$ electron transfer is slower ($b1_d = 2000$) than the second electron transfer ($b2_d = 5000$ s^{-1}). This is a critical requirement because the J inflection disappears when the rate constant values are reversed, and the first electron is transferred faster than the second ($b1_d = 5000$, $b2_d = 2000$ s^{-1}, Fig. 4b). The level of the J inflection decreases and a dip appears when electron donation from the S-states becomes rate limiting ($j_d = 3000$ s^{-1}, Fig. 4c). With this j_d value, the depth of the dip was still smaller than in experiments (Fig. 1 in Schansker et al. 2011), but j_d of 2000 s^{-1} (donation time 0.5 ms) gave a deeper dip. The strong donor side limitation, however, lowered the height of the J inflection significantly under the experimental value of 0.6 F_m (Fig. 4d).

A limitation of the current model is negligence of the different electron donation times from S-states advancing during the induction. A qualitative exploration of this process appears in panels A, C, and D of Fig. 4. During the transfer of the first electron (S_1 state), fluorescence follows the trace in panel A (actually to the somewhat lower J level, but the overly fast $j_d = 100{,}000$ s^{-1} was chosen to ensure the presence of the J inflection independent of donor side processes). When the second electron is transferred with $j_d = 3000$ s^{-1}, the fluorescence curve shifts from that in panel A to that in C, describing a dip actually deeper than visible in C. The latter dip could be even deeper due to slower donation from the S_3 state, but a mixture of S-states in the leaf may dampen the transition.

Summarizing this section, the J inflection is not a straightforwardly interpretable phenomenon, but its basis is a complicated balance between donor and acceptor side electron transfer rates within PSII. Even without donor side limitation, at the J level Q_A is reduced only in 70% of PSII units, and in a still smaller fraction when the donor side is rate limiting. Fluorescence remains briefly constant at the J level, while the fraction of forms with Q_A reduced remains constant as well. This occurs when the rate of $Q_A^- \rightarrow Q_B$ transfer is equal to the rate of Q_A reduction by photochemistry. At lower PFDs, this balance occurs with a smaller fraction of Q_A reduced, corresponding to a lower J-level fluorescence. The J level increases with increasing PFD provided that electron availability from the Mn complex is non-limiting. In the contrary case, i.e., light saturation due to the donor side limitation, the latter determines the maximum J level which may be lowered due to quenching by accumulation of $TyrZ_{ox}$ and $P680^+$. In this case, application of a STF does not increase J-level fluorescence (Schreiber et al. 2012). The J inflection is pronounced when the transfer of the second electron is faster than that of the first electron, blending into a more or less constant balance between electron arrival to and departure from Q_A. On the other hand, when the first electron is transferred faster than the second electron, equilibration of Q_A^- with the Q_B pool by the first electron occurs at a lower J level than that by the second electron, generating a continuously increasing fluorescence transient. The dip (D level) after the J inflection is generated when the second electron is transferred much faster than the first, and is enhanced when the forms with oxidized donor side carriers $Y_oP_oA_o$, $Y_oP_oA_r$, and $Y_oP_rA_o$ strongly quench fluorescence. Their combined fraction is small, but enough to cause the temporary dip in fluorescence. These fractions not only deepen the dip, but also quench the height of the J inflection below the experimental level of Schansker et al. (2011). A compromise parameter value for fitting to the experiment would be $k_r = 0.5$, for which the flash fluorescence $F_f = 0.66$ F_m. The following calculations use this k_r value and $b1_d = 2000$ and $b2_d = 5000$ s^{-1}.

Plastoquinone reduction

Plastoquinone reduction is a kinetically complex process involving exchange between free PQ and PQH_2 pools and an empty Q_B site. To investigate the process, the initial (dark) condition was set to $Y_rP_rA_oB_{oo} = 1$ (all PSII bound with PQ in the Q_B site) and the additional free pool PQ = 4 per PSII. Thus, there are altogether 5 PQ per PSII, initially all oxidized. Light intensity was set high,

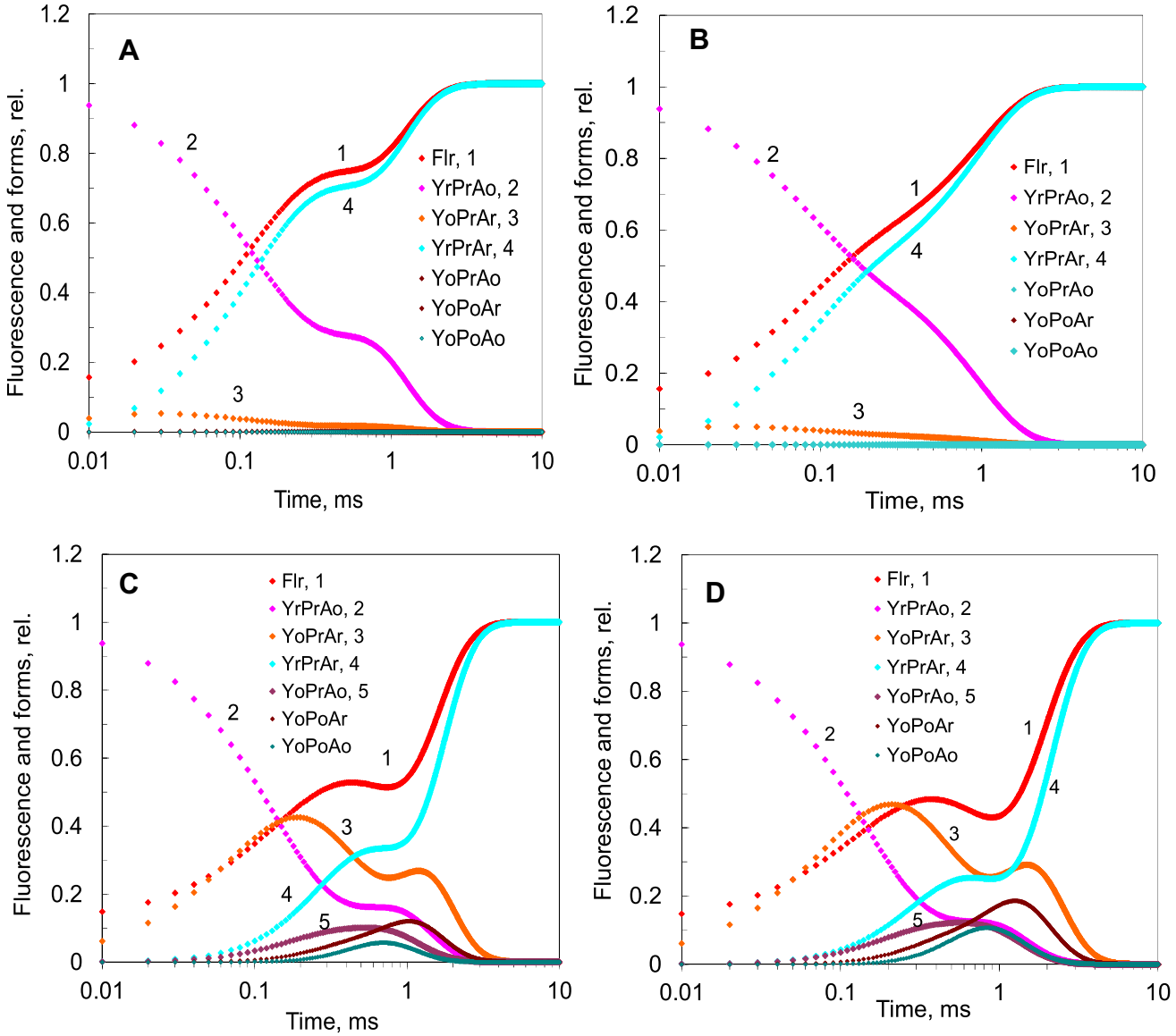

Fig. 4 In these panels, Q_B reduction by Q_A^- was activated, but Q_B exchange with free PQH_2 and PQ pools was forbidden by setting the rate constants $rq_d = oq_d = rq_r = oq_r = 0$. Plotted are fluorescence yield (red line) and groups of forms with Y, P, and A reduction state as indicated. Each of these represents the sum of four forms—with empty Q_B site, with B_{oo}, B_{ro}, and B_{rr}. PFD = 15,000 μmol m^{-2} s^{-1} in all panels. Panel **a** j_d = 100,000 s^{-1} (no donor side limitation), $b1_d$ = 2000, $b2_d$ = 5000 s^{-1}. The J inflection appears independent of donor side limitation when $b2_d > b1_d$. Panel **b** j_d = 100,000 s^{-1} (no donor side limitation), $b1_d$ = 5000, $b2_d$ = 2000 s^{-1}. The J inflection disappears when $b2_d < b1_d$. Panel **c** j_d = 3000 s^{-1}, $b1_d$ = 2000, $b2_d$ = 5000 s^{-1}; the dip after the J inflection is related to donor side limitation. Panel **d** j_d = 2000 s^{-1}. The dip deepens with stronger donor side limitation, but the height of the J inflection decreases too

PFD = 15,000 μmol m^{-2} s^{-1}, to match the fastest induction curve in Fig. 1 of Schansker et al. (2011). Oxidation of PQH_2 by Cyt b_6f was blocked by setting the rate constant $k_{b6f} = 0$. In accordance with the common understanding that "reduced quinone is released from, but oxidized quinone replaces it in the Q_B site," the rate constants were set at $rq_d = oq_r = 2000$, while the reversal rates were set at $rq_r = oq_d = 100$ s^{-1} (note that the "direct" rate is defined as away from PSII). The resulting induction curve did not resemble the experimental curve at all (Fig. 5a, red line). The reason was the large equilibrium constant between Q_A and PQH_2, preventing Q_A reduction before PQH_2 becomes highly reduced (Fig. 5b). To prevent the redox equilibration between PQH_2 and Q_A, the binding and unbinding rate constants were set such that about equal occupancy of the Q_B site by both ligands was ensured at their medium reduction level (Crofts and Wraight 1983; Robinson and Crofts 1983). The absolute values of 2000 s^{-1} ensured fast exchange of quinone between PSII and Cyt b_6f within 1 ms (Laisk et al. 2016), but the second-order rebinding rate constant of 2000 s^{-1} per PQH_2 ensured

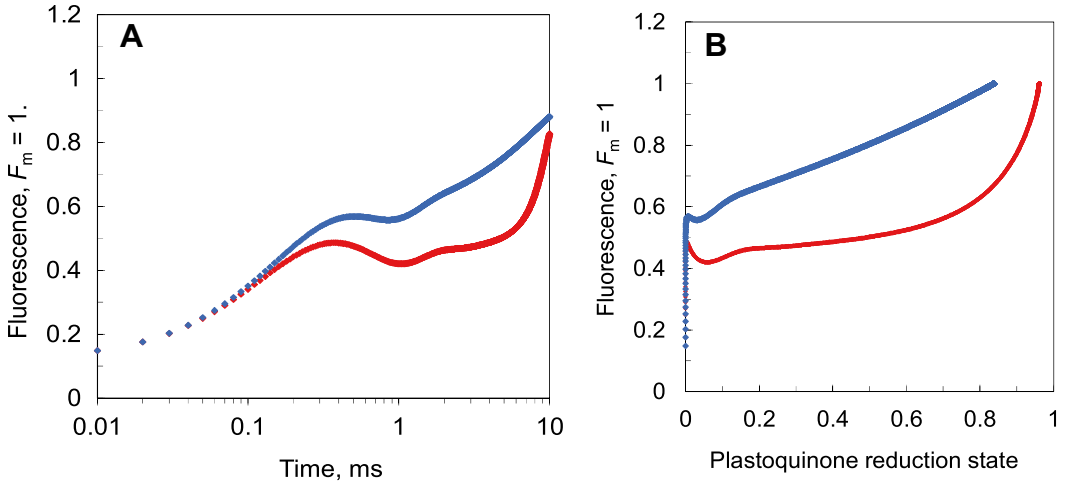

Fig. 5 The exchange of PQH_2 and PQ with the Q_B site was activated, but oxidation of PQH_2 by Cyt b_6f was blocked by setting k_{b6f} = 0. PFD = 15,000 µmol m^{-2} s^{-1} j_d = 3000 s^{-1}, $b1_d$ = 2000, and $b2_d$ = 5000 s^{-1}. Red lines rq_d = 2000 s^{-1}, rq_r = 100 s^{-1} per PQH_2 per PSII, oq_r = 2000 s^{-1} per 1 PQ per PSII, oq_d = 100 s^{-1} ("direct" means away from PSII). Blue lines rq_d = 2000 s^{-1}, rq_r = 2000 s^{-1} per PQH_2 per PSII, oq_r = 2000 s^{-1} per 1 PQ per PSII, oq_d = 2000 s^{-1}

sufficient competitive rebinding of PQH_2, particularly at its higher reduction levels, when PQH_2 = 2 to 4, but PQ is low. With these rate constants, the modeled approach of fluorescence to F_m was rather similar to the experimental trace in the log time axis (Fig. 5a, blue line). As expected, fluorescence yield increased about proportionally with increasing PQ reduction (Fig. 5b, blue line). This is caused by product inhibition by PQH_2 of PSII as the water–plastoquinone reductase, due to fast re-association of PQH_2 with the Q_B site. Naturally, the I inflection is still absent in this transient, since PQH_2 oxidation is blocked.

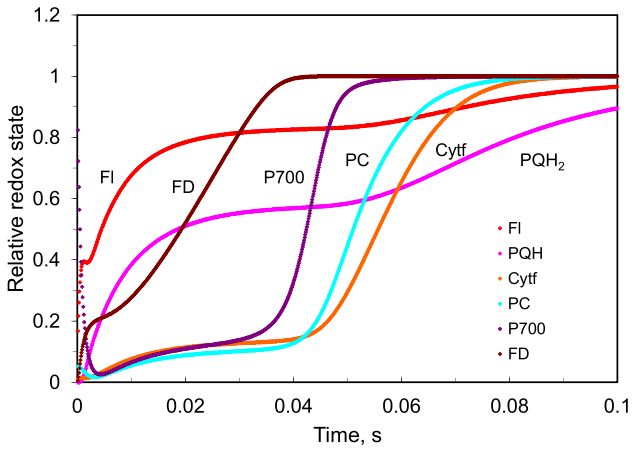

Fig. 6 Reduction state of electron carriers during a full induction. PFD = 3000 µmol m^{-2} s^{-1}, other parameters as in Table 1

Full induction

Mathematical description of the full induction requires modeling of electron transport through the Q-cycle and through PSI. The last processes are not reflected by Chl fluorescence in such detail as the PSII kinetics. Therefore, here we neglect the master-equation approach (see Lebedeva et al. 2002), but apply ordinary differential equations to describe the reduction–oxidation budgets of individual carriers, despite the fact that some of them occur within a common protein complex.

Fluorescence induction from the dark-adapted state is a dead-end process, where electron transport is blocked beyond ferredoxin—most likely caused by reversal of GAP-dehydrogenase in the dark, leading to over-reduction of NADPH. As light is turned on, electrons are transported from the PSI donor side to its acceptor side, accumulating in FD, but leaving the donor side carriers ready to accept electrons generated by PSII. Ferredoxin becomes reduced first, followed by P700, PC, Cyt *f*, and PQH_2 (Fig. 6). The induction lasts until all electron carriers become reduced, ending with F_m-level fluorescence.

The set of induction curves modeled with the rate constant of PQH_2 oxidation k_{b6f} of 50 s^{-1} exhibits the I inflection at 20–50 ms (Fig. 7). In order to slow down the whole transient in accordance with the experiment (Schansker et al. 2011), the product inhibition of PSII by PQH_2 was increased by setting rq_r = 5000 s^{-1} per 1 PQH_2 per PSII. The characteristic light dependence of the I level is caused by the first-order kinetics of the Q-cycle reactions—the level of PQH_2 increases proportionally with the electron transport rate, but fluorescence in its turn increases in proportion with the PQH_2 level. At very high PFDs, the PSII

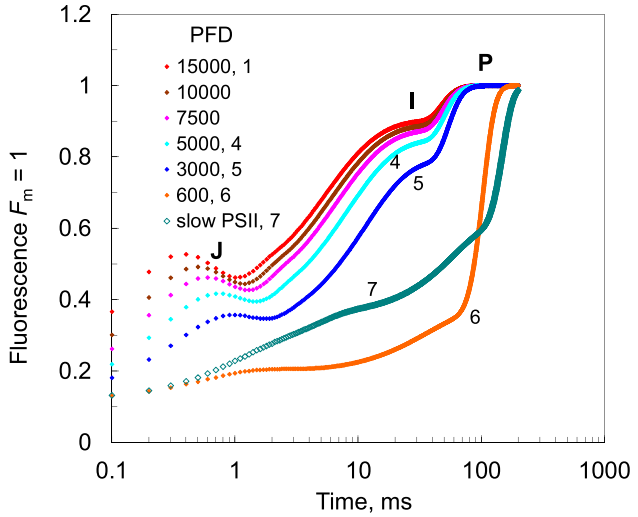

Fig. 7 Full inductions with different light intensities. j_d = 2000 s^{-1}, rq_d = 2000 s^{-1}, rq_r = 5000 s^{-1} per 1 PQH_2 per PSII, oq_r = 2000 s^{-1} per 1 PQ per PSII, oq_d = 2000 s^{-1}, k_{b6f} = 50 s^{-1}, other constants as in Table 1. The "slow PSII" curve was calculated with $b1_d$ = 1000 and $b2_d$ = 500 s^{-1}

donor side becomes rate limiting, determining the highest I level saturated with respect to the light intensity. At PFDs down from 15,000 to 3000 µmol m^{-2} s^{-1}, the shape of the calculated FI curves is in accordance with those in Fig. 1a of Schansker et al. (2011) measured in pea leaves, but at lower PFDs the calculated curves did not match the measurements of Fig. 1b of the same study carried out with tobacco leaves. The calculated example at a PFD of 600 µmol m^{-2} s^{-1} stays at the low fluorescence <0.3 F_m until 50 ms, but the measured curve increased to about 0.6 F_m at the same time.

Literature reports indicate that considerable differences can occur among different plant species in antenna size, PQ pool size, etc. But PSII core structure is highly conserved. Nevertheless, the too fast initial rise of fluorescence between 0.1 and 10 ms at low light intensity suggests decreased or downregulated electron transport within PSII, but not beyond it. This assumption was confirmed by the trace calculated for the PFD of 600 µmol m^{-2} s^{-1} with $b1_d$ = 1000 and $b2_d$ = 500 s^{-1}, fitting the corresponding curve in Fig. 1b of Schansker et al. (2011).

The K peak in heat-treated leaves

Even a brief exposure to >45 °C destroys the Mn complex, resulting in a drastic change in FI curves: the J and I steps disappear, but a novel K peak develops at 300–400 µs at high PFDs (Tóth et al. 2007a). This K peak was suggested to be related to oxidation of TyrZ and is thus a suitable candidate for modeling donor side oxidation.

The heat-inhibited FI transient was modeled with the same set of constants as in Fig. 7, except that the donor rate j_d was decreased from 2000 to 200 s^{-1} (Fig. 8). The slow residual water-splitting activity was retained to simulate electron donation from stromal reductants. The K peak is indeed produced, but like the J inflection it is not directly related to oxidized TyrZ. The forms containing Y_o together approach 50% at 0.6–0.8 ms, the rest remaining in the initial state $Y_rP_rA_o$. Soon after the K peak, fully oxidized $Y_oA_oP_o$ dominates, decreasing fluorescence to the minimum due to quenching by $P680^+$.

This model does not reproduce the P peak as recorded in Tóth et al. (2007a), probably because ferredoxin-NADP reductase is not activated in the model, but could become activated in experiments, where the recording is extended to 1 s. If this happened, fluorescence decreased, because the ET chain became re-oxidized. Re-activation of ferredoxin-NADP reductase could be facilitated by ascorbate, as observed in the experiments of Tóth et al. (2007a).

Fluorescence and electron transport rate

Occupancy (presence) of the donor-oxidized forms of PSII is significant during the initial phase of induction, when total electron transport rate is fast. Each of these YPA forms (Fig. 9) is the sum of four forms—YPA without B (empty Q_B site), $YPAB_{oo}$, $YPAB_{ro}$, and $YPAB_{rr}$. We reiterate that fluorescence yield was defined differently depending on the reduction state of YPA, but independent of B (Eq. 38). Fluorescence is initially at the F_o level in $Y_rP_rA_o$ forms; it is at the flash F_f level in $Y_oP_rA_r$ forms after one electron is transferred and approaches the F_m level when all the three become reduced ($Y_rP_rA_r$). Transient double

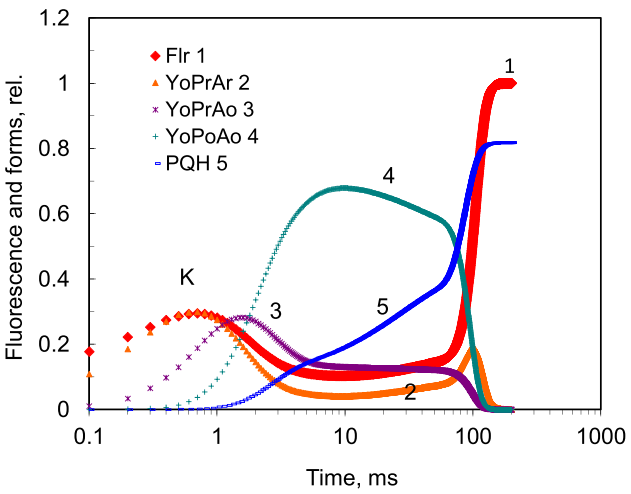

Fig. 8 Full induction reproducing the K peak when the water-splitting complex was inhibited by setting j_d = 200 s^{-1}. PFD = 3000 µmol m^{-2} s^{-1}, other parameters as in Fig. 7

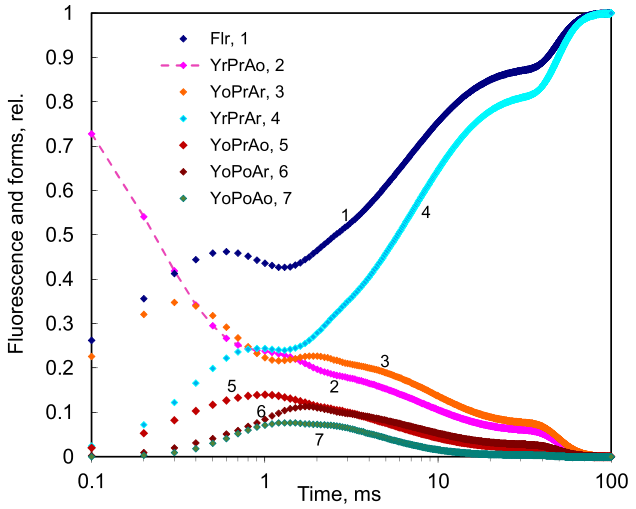

Fig. 9 Time courses of different PSII forms during full dark–light inductions of fluorescence. Each of the indicated forms is a sum of four "subforms"—with empty Q_B site, with B_{oo}, B_{ro}, and B_{rr}. PFD = 7500 μmol m^{-2} s^{-1}, other parameters as in Fig. 7

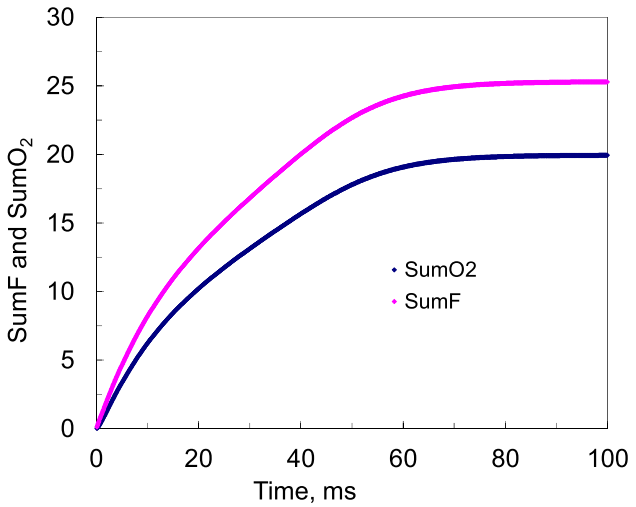

Fig. 10 Number of electrons transported per PSII during an induction, calculated as an integral donated by the S-states ($SumO_2$, Eq. 37) and an integral of quenched fluorescence (SumF, Eq. 39). PFD = 3000 μmol m^{-2} s^{-1}, other parameters as in Fig. 7

oxidation of the donor side is assumed possible, occupying $Y_oP_oA_r$ and even $Y_oP_oA_o$ forms—each up to 10% at a PFD of 7500 μmol m^{-2} s^{-1}—emitting very low fluorescence (Eq. 38). During the first milliseconds of illumination, the occupancy of the $Y_rP_rA_o$ form rapidly decreases (note the rare diamonds), being substituted mainly by $Y_oP_rA_r$, but other electron transfers occur simultaneously: S-state→Y_o transfer creates $Y_rP_rA_r$ emitting at F_m, Q_A→Q_B transfer creates $Y_oP_rA_o$ emitting at $<F_o$, but double oxidation of the donor side inhibits $Y_oP_oA_r$ and even $Y_oP_oA_o$ forms emitting at very low level due to strong quenching by $P680^+$. Accumulation of these strongly quenching forms causes the dip past the J inflection at around 1–2 ms of induction. All these donor-oxidized forms remain present during the whole induction, though their occupancy gradually decreases as the electron transport rate decreases. This explains why the true F_m can be reached only after the complete reduction of the whole electron transport chain—because the donor ($TyrZ_{ox}$ and $P680^+$) and acceptor side (Q_A) quenching disappears only when electron transport rate decreases to zero.

Accumulation of the fluorescence-quenching but not electron-transporting donor-oxidized forms leads to a discrepancy between integrated electron transport calculated from fluorescence and O_2 evolution (Eqs. 37 and 39). During an induction at PFD = 3000 μmol m^{-2} s^{-1}, 20 electrons per PSII were transferred during the whole induction as detected from O_2 evolution (an integral of the S-state to Y_o electron transfer rate in the model, Eq. 37), but 25.3 electrons were calculated from fluorescence quenching (Fig. 10). This overestimation is small at low PFDs, but increases with increasing light intensity (Fig. 11a). Such a dependence is analogous to a counter of photons operating with a dead time, like a Geiger–Müller counter of nuclear particles:

$$n = \frac{n_0}{1 + n_0\tau}, \tag{40}$$

where n is the number of counted particles, n_0 is the actual number of particles hitting the counter, and τ is the dead time—the time interval after each successful hit during which the detector does not respond. During photosynthesis, photons exciting PSII are the incident particles and transferred electrons are the actual "counted" ones, but τ is the time interval after each electron transfer, during which the exciting photons are missed, which can be expressed using Eq. (40) as

$$\tau = \left(\frac{n_0}{n} - 1\right)/n_0, \tag{41}$$

where n_0 is SumF—the number of transferred electrons calculated from fluorescence quenching—and n is $SumO_2$—the number of transferred electrons donated from the S-states. The ratio n_0/n is unity at low PFDs, but non-linearly increases with increasing PSII excitation rate (Fig. 11a). The non-linearity translates into increasing τ, beginning with 0.1 ms at low PFDs and approaching 0.25 ms at the highest PFD of 10,000 μmol m^{-2} s^{-1} ($n_2 = 4.86$ ms^{-1}). This non-linearity is caused by the "buffering effect" due to the dual oxidation on the donor side. Electron donation rate to TyrZ was constantly set at 2000 s^{-1}, but due to the allowed dual oxidation on the donor side two electrons could be transferred before PSII became closed on the donor side. This was more likely to happen at high than at low PFDs. This

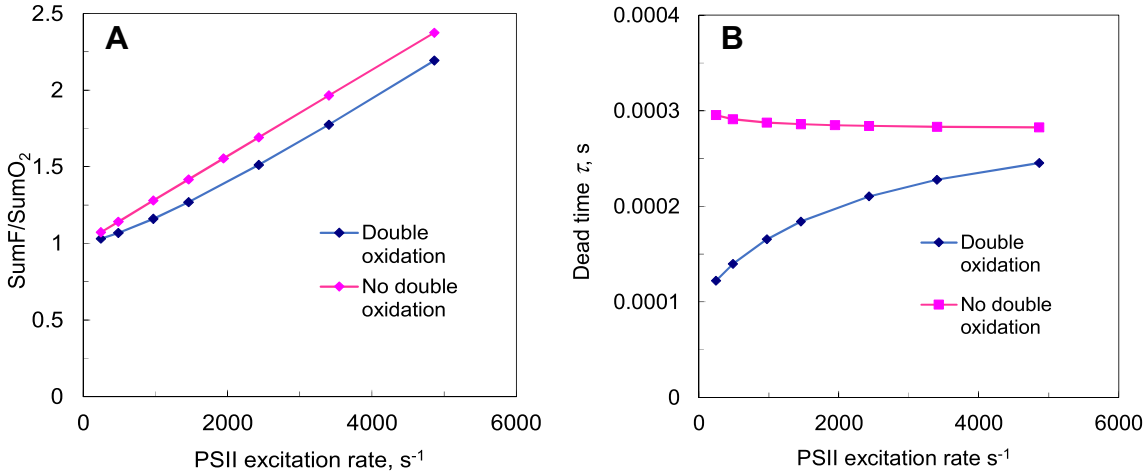

Fig. 11 Overestimated electron transport from fluorescence quenching. Panel **a** $SumF/SumO_2$ dependent on the PSII excitation rate (parameters as in Figs. 7, 9, 10), Panel **b** The corresponding dead time τ. Blue lines indicate the values calculated assuming the possibility for double oxidation of the donor side ($P680^+$ may accumulate), and red lines indicate the values calculated assuming no electron transfer in PSII with oxidized TyrZ (no accumulation of $P680^+$)

condition was tested by forbidding light-induced electron transfer from all $Y_oP_rA_o$ forms in the model, though P680 was reduced and Q_A was oxidized—resulting in constant τ of 0.28 ms instead of 0.5 ms as defined by $j_d = 2000$ (the reason for this apparent discrepancy is the preset fluorescence yield of 0.66 F_m for the tyrosine-oxidized PSII units, which only partially reflected the donor-blocked electron transfer in fluorescence quenching).

Discussion

Scientific output of modeling

The model *program* was created in accordance with our best *notion* about the photosynthetic electron transport. The computation results are thus expected to mimic the dynamic features of photosynthesis. If successful, the work would confirm that the *program* is close to the *notion* and the latter is close to *Nature*—how the process actually occurs. Thus, more interesting are cases when the computed results differ from the actual data. A valid caution is vigilance for limitations in the *program*. An evident deficiency of our program is the neglected dependence of electron donation rate on the number of S-states, which we attempted to ease by mixing *computing* and *thinking* (Fig. 4). But could it be that the present *notion* taken for the basis of the *program* is wrong or insufficient itself? We reject the case that the Z-scheme is wrong in its general structure, but how about details—like values of some rate constants? For the sake of better coincidence with experiments, we had to use a partially quenched fluorescence value $F_f < F_m$ for PSII with reduced Q_A but oxidized Tyr Z—not recognized in the common *notion*. In order to reproduce the J inflection, we needed to use an electron transfer rate constant slower for the $Q_A^- \rightarrow Q_B$ and faster for the $Q_A^- \rightarrow Q_B^-$ transfer—in contradiction to some literature reports. In order to reproduce the linear (on a logarithmic scale) rise of fluorescence between the J and I inflections, we needed to use a higher empty Q_B site affinity for PQH_2 than for PQ—suggesting a strong product inhibition of PSII by reduced plastoquinone not appreciated before. These novel, yet testable, observations invite confirmatory efforts using alternate methodologies.

Usually, model rate constants are based on experiments with isolated chloroplasts, thylakoids, or enzymes, believed to be more direct and reliable than fittings of kinetics with intact leaves. On the other hand, a fluorescence induction trace measured on an intact leaf is also an informative experiment, despite the necessity of computation to evaluate rate constants. Calculations are needed to express the characteristic constants even in in vitro studies. A relevant example is the measurement of electron transport rate from Q_A^- to Q_B and Q_A^- to Q_B^- in a frequently cited work (de Wijn and van Gorkom 2001). The study involved the measurement of Chl fluorescence yield decay after laser flashes in a series of advancing S-states and altered Q_B reduction state. In thylakoids isolated from spinach leaves (de Wijn and van Gorkom 2001), as well as in chlorella cells (Kolber et al. 1998) and leaves of different plant species (Osmond et al. 2017), the post-flash decay of chlorophyll fluorescence yield appeared to be highly polyphasic, with only slight differences between the flashes. Deconvolution of the data from the mixture of S-states and correction for

the non-linear dependence of fluorescence yield on the concentration of Q_A^- for excitonic connectivity between PSII units were required. As a result of such sophisticated mathematical modeling and application of advanced statistical procedures, two kinetic components could be distinguished in the oxidation of Q_A^- with time constants in the range of 0.2–0.8 and 2–3 ms, respectively, in addition to a minor, much slower component. An original report (Bowes and Crofts 1980) that Q_B is reduced faster than Q_B^- could be confirmed only conditionally: the fastest time constant of 0.2 ms covered only a part of the Q_B reduction transient, but the overall fluorescence decay was actually slower than that for the Q_B^- reduction—due to the presence of a slow decay phase that occurs on Q_B, but not on Q_B^-, reduction. In our work, the J inflection could be reproduced when Q_B was reduced within 0.5 and Q_B^- within 0.2 ms, slower values being clearly insufficient to cope with the fast electron transport at light intensities above 3000 µmol m^{-2} s^{-1}. Such a result is even expected in the sense of the quinone stability: while one electron is shared between the Q_A and Q_B semiquinones, its stabilization on Q_B^- with an equilibrium constant (kE_1) of ~20 is determined by protein environment. As soon as the second electron arrives, the very stable Q_B quinol rapidly and strongly binds both electrons (de Wijn and van Gorkom 2001). Since the J inflection is a strong experimental fact, we used the rate constants $b1_d = 2000$ for the first and $b2_d = 5000$ s^{-1} for the second electron. The dip after the J inflection was due to strong quenching by forms with oxidized P680 and/or oxidized TyrZ; $Y_oP_oA_o$, $Y_oP_oA_r$, and $Y_oP_rA_o$.

Thus, the application of *computing* to the experimental curves is a logically correct—and actually widely used—way of obtaining scientifically novel results. Usually, a limited number of parameters are related to a particular kinetic feature, so that the fear of multiple equivalent solutions is exaggerated.

Thermal phase of fluorescence induction—the *notion*

We have shown that the "thermal phase" of fluorescence rise kinetics is explained by gradual relaxation of two types of quenching—photochemical quenching due to oxidized Q_A and donor side quenching due to photo-oxidized TyrZ and P680. The observed fluorescence is a sum of emission from individual PSII units: some are at state F_o, some at F_m, some at F_f, and some quenched to about zero. Total electron transport rate through PSII gradually decreases during the fluorescence rise, but this smooth decline is an average, not reflected in each PSII unit—electron transport is still maximal in units with oxidized Q_A and reduced donor side, but becomes zero in PSII where Q_A is reduced or the donor side is oxidized. At the beginning of FI, the forms emitting at F_o dominate. The first electron transfer to Q_A generates $TyrZ_{ox}$, but in our time-scale leaves P680 unoxidized, the form assumed to be emitting at F_f. Secondary donation from the S-states reduces the $TyrZ_{ox}$, generating a fraction of PSII units emitting at F_m. Simultaneous electron transfer to Q_B re-oxidizes Q_A^-, restoring emission at the F_o level. Forms of PSII emitting at the F_o level and at the F_f level gradually disappear, while the forms emitting at the F_m level become dominant. At very high PFDs, the model allows double oxidation of the donor side, transiently accumulating a form with $TyrZ_{ox}$ and $P680^+$, emitting at a level about zero. This complex understanding was facilitated by prior mathematical modeling applying techniques of master equations (Paillotin et al. 1983; Lebedeva et al. 2002; Lazár 2003), but developed further in this work by differently grouping intrinsic electron transfer steps within PSII. It is worth noting that the first-order reactions describing conversions between the PSII forms are actually exponential functions with the given time (or rate) constants. Due to this, the initially synchronized forms rapidly become mixed, e.g., if the S-state donation time constant is 0.2 ms, then at this time only 0.74 of all flash-oxidized TyrZ have become re-reduced.

Our effort is offered with an eye to general scientific progress, i.e., no model is above being revisited. Contemporary information about PSII structure and function discerns too many kinetically complex electron transfer steps to be realistically described with a system of master equations. This brings us to the problem of optimal simplification, as different approaches lead to different simulation results (Lazár and Jablonsky 2009). In the present model, we combined the reversible charge-separated states, $Pheo^-$ and P_{D1}^+ (or Chl_{D1}^+), into one vibrationally coherent complex P680. In this denotation, P680 is the "six-pack" complex of P_{D1}·P_{D2}·Chl_{D1}·Chl_{D2}·$Pheo_{D1}$·$Pheo_{D2}$ (Renger 2010). Our basic assumption is that exciton localization on P_{D1}·P_{D2}·Chl_{D1}·$Pheo_{D1}$ of this complex, specifically the $Pheo_{D1}^-$ ·P_{D1}^+ intermediate charge-separated state, is in equilibrium with excitation on the antenna pigment complex (Novoderezhkin et al. 2015). Excitation is photochemically quenched only after an electron is stabilized on Q_A. The earlier assumption that charge recombination between $Pheo^-$ and P_{D1}^+ dissipates excitation caused problems in the study of Lazár (2003), which did not reproduce period-four oscillations in flash O_2 evolution, and for Belyaeva et al. (2011), who reported a significant influence of membrane potential and lumen acidification on PSII charge transfer efficiency during induction. If P680 would have been considered as the above "six-pack" or "four-pack" (Novoderezhkin et al. 2015) and the state with $TyrZ_{ox}$ as a normal long-lived form of PSII, then the mysterious "intermediate S-states" (Jablonsky and Lazar 2008) would have been unnecessary.

As reported in this work, earlier models sought to reproduce the fluorescence rise with its OJDIP inflections. The mass action linear approach—equivalent to expression

as a sum of exponentials (Strasser and Govindjee 1991; Strasser et al. 2004; Vredenberg 2008a, 2015)—has qualitatively resolved the characteristic sub-processes, laying the base for a series of reports culminating in computer-calculated parameters by a commercial photosynthesis efficiency analyzer (PEA). The master-equation approach was developed to its apotheosis in Lebedeva et al. (2002), Belyaeva et al. (2006), and Lazár (2003). How was it possible that these models reproduced the light-dependent induction curves with their J and I inflections without incorporation of the novel features we introduced in this study? The low flash fluorescence was actually ignored by these models and the J inflection was generated and explained as follows. "Phase J is clearly discerned only under intense enough light, and is associated with accumulation of fluorescing states in which the acceptor is not fully reduced (not more than one electron on Q_B)" (Lebedeva et al. 2002). "J step is caused by the superposition of the accumulation of excited states that are formed when only Q_A is reduced, or when Q_A is reduced together with singly reduced Q_B" (Lazár 2003). These statements demonstrate a frequent problem: a *program* may succeed in mimicking the natural process, but the verbal explanation of its internal relationships—*notion*—may be different. Above the PSII form with Q_A reduced was stated to emit fluorescence at the J level, but why not at the F_m level? Also how can an electron on Q_B partially quench fluorescence to the J level? In this work, we aimed to promote the understanding of fluorescence emission in terms of PSII electron transport kinetics.

During the J inflection, fluorescence remains briefly static as electron arrival to and departure from Q_A remain equal, resulting in constant occupation of the Q_A^- form at an average reduction level of about 0.7 at the high light intensity (Fig. 4). The arrival rate depends on light intensity, but it approaches a ceiling limited by donation from the S-states. The departure rate depends on the $Q_A \rightarrow Q_B$ transfer. As discussed above, de Wijn and van Gorkom (2001) revealed the complex nature of this process—the first electron reducing Q_B initially faster, but the whole process being slower than the single exponential reduction of Q_B^- by the second electron. Our modeling confirms that with the time constants of 0.2 for the first and 0.5 ms for the second electron the J inflection did not appear (Fig. 4b), because the equilibrium Q_A^- occupancy was lower for the first than for the following second electron, continuously rising with time due to the mixing of forms. Contrary to this, the J inflection was pronounced when the transfer of the second electron was set faster than that of the first electron, blending the two rates into a more or less constant balance between the arrival and departure of the two electrons (Fig. 4a). Notably, these kinetics were expressed while Q_A and Q_B became reduced within PSII, without exchange with free PQ. Such a test computation was not shown by Lazár (2003, 2009), Lebedeva et al. (2002), or Belyaeva et al. (2011). Therefore, in these models the temporarily balanced Q_A^- state during the J inflection involved the $Q_A \rightarrow Q_B$ as well as the $Q_B \rightarrow PQ$ electron transfer. In our hands, a similar computation resulted in Fig. 5a—an over-pronounced J inflection and D dip lasting while the PQ pool became almost fully reduced. This happened because the gradual accumulation of PQH_2 had no feedback to Q_A reduction, due to the extremely large equilibrium constant between the semiquinone and quinol. In order to eliminate such an evidently incorrect response, PQH_2 was assumed to be able to reduce Q_A to some extent and fluorescence quenching by oxidized plastoquinone was assumed (Lazár 2003, 2009). Although possible in thylakoids, this process is not present in leaves (Tóth et al. 2005b). In this work, we suggest a mechanistic process instead of "quenching by oxidized plastoquinone"—competitive binding of reduced plastoquinone to the Q_B site.

An important electron transfer step is equilibration of the Q_B site with diffusible PQH_2 and PQ species, explicitly modeled in this work compared to Lazár (2009). Although sometimes diffusion of the quinone species is considered rate limiting for photosynthesis (Lavergne and Joliot 1991; Joliot et al. 1992; Kirchhoff et al. 2000; Haferkamp et al. 2010), our recent work on intact leaves showed very fast equilibration (within less than 1 ms) of the diffusible quinone species with the Q_B site on one hand and with the primary quinone binding p-site of Cyt b_6f on the other hand (Laisk et al. 2016). In accordance with this, the rate constants for dissociation of PQH_2 from the Q_B site (rq_d = 2000 s^{-1}) and association of PQ with the Q_B site (oq_r = 2000 s^{-1} per PQ = 1 per PSII) were set fast. The common understanding that PQH_2 is always rapidly exchanged for PQ in the Q_B site did not work, since the calculated induction trace was strongly sigmoidal, expressing a very long J inflection in the log scale, significantly different from the experimental one (Fig. 5). A better result was obtained when fast re-association of PQH_2 with and dissociation of PQ from the Q_B site were allowed, in accordance with the notion that neither quinone nor quinol bind tightly (Crofts and Wraight 1983): $Q_BH_2 + PQ \leftrightarrow Q_B + PQH_2$, $K_3 = 1$. In order to fit the calculated induction trace to the measured one, the PQH_2 re-association rate constant rq_r had to be set at least equal to or even faster (rq_r = 5000 s^{-1} per PQH_2 = 1 per PSII) than its dissociation rate constant (rq_d = 2000 s^{-1}). Initially, the high affinity of the Q_B site for reduced PQH_2 was detected from light pulsing experiments in intact sunflower leaves. When PQ was reduced illuminating a leaf with gradually longer multiple-turnover light pulses, the rate of PSII electron transport decreased proportionally with the decreasing fraction of oxidized PQ. Such apparently linear kinetics with respect to PQ, earlier detected from fluorescence

measurements (Tóth et al. 2007b), were suggested to be caused by strong product inhibition by PQH_2, blocking the Q_B site for electron transfer in proportion with its pool size (Oja et al. 2011; Laisk et al. 2015). As a result, fluorescence yield is rather proportional to PQH_2 reduction state during induction (Tóth et al. 2007b; Fig. 5b).

This kinetic property explains the peculiar discrepancy in temporal courses of fluorescence induction (Tóth et al. 2005a; Laisk et al. 2015; Schansker et al. 2011). When light is turned on for the first time, fluorescence rise is slow, approaching F_m during a light pulse of about 200 ms. In the dark after the pulse fluorescence decreases initially faster, but approaches a low value of about 2 F_o within a few seconds. When the light is turned on again, fluorescence approaches F_m within a millisecond, quite like in DCMU-treated leaves. In kinetic terms, the result indicates that after the pulse PQH_2, and in equilibrium with it Q_B, remains reduced for a longer time, but Q_A becomes oxidized, probably due to charge recombination—despite the fact that Q_B is occupied by PQH_2. When light is turned on again, the re-induction of fluorescence is fast, as with DCMU.

PQH_2 oxidation by the Q-cycle in the Cyt b_6f complex is the major rate-limiting event in photosynthetic electron transport. Although a complex process involving two oxidations of PQH_2 and one reduction of PQ, its overall kinetics are equivalent to two first-order reactions in series, the first being faster and the second slower (Laisk et al. 2016). In the present approach, complete PQH_2 oxidation was modeled with a single first-order rate constant of 50 s^{-1}—the sum of the two component reaction times. It must be emphasized that the frequently cited rate of post-illumination reduction of P700 and PC of about 100 to 200 s^{-1} is not the rate constant of PQH_2 double oxidation, but involves the pool sizes of P700 and PC, but each possessing one redox electron. During induction, the Q-cycle rate gradually decreases, being limited by the availability of the electron acceptor, oxidized Cyt *f*. Thylakoid membrane potential may also participate in this process (Lebedeva et al. 2002; Belyaeva et al. 2011), but during the relatively fast fluorescence rise its role is indistinguishable from that of the gradually reducing electron acceptors. Neglecting master equations for the Cyt b_6f complex and PSI complex (see Lebedeva et al. 2002) could cause inaccuracies in calculating the true reduction states of Cyt *f*, P700, and the PSI acceptor FX (a formal denotation, not necessarily the corresponding FeS complex), but this could hardly be reflected in the corresponding PSII fluorescence traces.

Similarity of the calculated traces to the measured curves (Schansker et al. 2011) confirmed that the kinetic characteristics of electron transport employed and their assumed relationship to Chl fluorescence are realistic. This proves that electrochemical quenching due to membrane potential difference (Vredenberg et al. 2009) and control of transmembrane charge transfer by membrane potential (Lebedeva et al. 2002; Belyaeva et al. 2006, 2011), which were omitted from our model, do not significantly control PSII electron transport and fluorescence emission during the dark–light fluorescence rise, at least at high light intensities. Most kinetic phenomena considered unexplainable in the framework of the Q_A model and requiring involvement of protein conformational changes (Schansker et al. 2011, 2014) are explainable as follows:

- A saturating single-turnover flash cannot generate more than 60–65% of the maximum fluorescence intensity and the J step is only 60–65% of the F_m value.

  We propose that oxidized TyrZ is related to quenching of the flash fluorescence F_f. The fast (within a microsecond) onset of this quenching during the ST flash cannot involve conformational changes. At the J step Q_A is partially reduced indeed.
- Electron flow through PSI has a kinetic effect on the Chl a fluorescence rise, i.e., a reduced electron transport chain is a pre-condition for reaching F_m.

  A reduced chain involves reduced plastoquinone. We propose that PQH_2 is a product inhibitor of PSII, binding competitively to the Q_B site. With highly reduced PQH_2, electron transport kinetically simulates inhibition by DCMU.
- Even high light of 15,000 µmol photons m^{-2} s^{-1} is not sufficient to eliminate the IP-phase.

  The I inflection level is lower than F_m because the balanced level of PQH_2 adjusts below its complete reduction. The rate of PQ reduction increases with light intensity, but the ceiling is donation by water splitting. This high PFD exceeds the maximum donation rate, and thus the I level becomes independent of light.
- The J step does not represent a single charge separation but 2–3 charge separations, and the J and I steps do not change position in response to changes in the light intensity.

  The J step appears as a temporarily stabilized Q_A reduction state, while electron donation by photochemistry and departure by $Q_A \rightarrow Q_B$ transition remain equal. The J step occurs while the first and second electrons are reducing Q_B, but may be extended if Q_BH_2 exchange with Q_B is fast enough. The J inflection does not change position because at low light the lower J level compensates for the shift to the right due to slow excitation. The I step is mainly determined by electron transfer kinetics from PSII to PSI, not photochemistry.
- The relaxation kinetics of the thermal phase, occurring within 100 ms, cannot be explained by any known redox reaction involving the re-oxidation of Q_A.

  If a process cannot be explained by any known redox reduction, then (a) a novel redox reaction has to be suggested or the rate constant of a known reaction modified or (b) a conformational change may be suggested.

We propose the modification of rate constants of charge recombination between Q_A^- and some S-states, rather than a conformational change relaxing faster than within a millisecond.

- The kinetics of the fluorescence rise at low temperatures do not agree with a photochemical reaction leading to the reduction of Q_A.

  Fluorescence rise kinetics rather similar to the experimental observations were modeled by assuming slow electron donation from an S-state at low temperature (Fig. 3).

The above arguments however do not mean that conformational changes accompanying PSII electron transport are excluded. The faster increase of the measured compared to the calculated fluorescence at low light intensities (Fig. 7) required light-dependent adjustment of kinetic parameters within PSII: the Q_A-to-Q_B transfer rates had to be decreased and Q_B reduction set faster than Q_B^- reduction. Notably, for the low-light FI curves the fitting $Q_A \rightarrow Q_B$ rate constants were 1000 for the first and 500 s^{-1} for the second electron, as appeared to be necessary to eliminate the low-level J inflection and ensure the continuous rise of fluorescence up to the I inflection at about 80 ms. Conditions and details of this phenomenon need further investigation and modeling, but it may just be the experimental indication of conformational changes controlling Q_A to Q_B electron transfer within PSII, as once suggested for bacterial photosynthetic centers (Xu et al. 2002). Another peculiar feature—the temporary decay upon darkening and fast recovery of fluorescence upon re-illumination—should promote further investigations of charge recombination from Q_A^- in the dark and Q_A re-reduction upon repeated illumination.

The present modeling approach was motivated by measurements showing significantly smaller rates of PSII electron transport based on O_2 evolution compared to fluorescence quenching (Oja et al. 2011; Laisk et al. 2012, 2015; Laisk and Oja 2013). According to these results, some of the fluorescence quenching must be of non-photochemical origin or related to non-oxygenic cyclic electron transport within PSII (Laisk et al. 1994). In most of the cited models, $P680^+$ was assumed to be the non-photochemically quenching species (for alternative suggestions see Introduction). Strasser (1997) explained the K step observable with damaged water-splitting complex (Fig. 8) in terms of accumulation of oxidized TyrZ, causing subsequent accumulation of $P680^+$ as the actual quenching form. Vredenberg (2008b) considered the possibility of fluorescence quenching by oxidized TyrZ, but could not find convincing arguments from experiments with DCMU-inhibited *Chenopodium* chloroplasts. Nevertheless, the amply documented period-four oscillation of the STF-induced variable fluorescence (Schreiber and Neubauer 1987; Kolber et al. 1998; Koblížek et al. 2001; Shinkarev 2004) was a strong argument for the S-state-related mechanism of diminished F_f fluorescence yield (Vredenberg 2008b).

The water-splitting complex becomes inhibited in leaves when exposed to temperatures exceeding 45 °C. Indeed, when temperature was gradually increased with a darkened leaf, fluorescence, initially at the F_o level, gradually increased to 0.5 F_m in the dark at temperatures >45 °C (Laisk et al. 1998). When saturation pulses were imposed on the same leaf, F_m was initially high but gradually decreased to a half at >45 °C—variable fluorescence disappeared. In this experiment, the yield of 0.5 F_m was adjusted in the absence of electron transport, when the q_E-type non-photochemical quenching was certainly absent. Therefore, it is very tempting to interpret this fluorescence yield as that of PSII with TyrZ being oxidized by the saturation pulse or by back-reaction to the damaged S-state in the dark.

Fluorescence yield, F_f, of flash-excited PSII units is about 3 to $3.5F_o$, while the F_m values are about 5 to $7F_o$ (Neubauer and Schreiber 1987; Samson and Bruce 1996; Vredenberg et al. 2007). In our calculations, the F_f yield was initially set at $0.5F_m$ (the DCMU calculations), but later increased to $0.66F_m$ based on the fit of the calculated J inflection level to the experimental curves. Instead of F_o, we used F_m as a natural fluorescence unit, because it is represented by a basic physical rate constant—the sum of excitation conversion rates to heat, triplet, and fluorescence—normalized to unity. F_o involves also the rate constant of photochemistry, which may vary depending on conditions. In well-conditioned leaves $F_m = 9F_o$ for the PSII fluorescence (Peterson et al. 2014), and therefore $0.5F_m = 4.5$, but $0.66F_m = 6\ F_o$. The fast response measurements of (Steffen et al. 2005) did not detect $TyrZ_{ox}$ as a quencher, but focused on Q_A, $P680^+$, and triplet ^{3}Chl (or ^{3}Car). But these authors overlooked that their maximum fluorescence F_m approached only $2F_o$ at 50 µs after the flash—when triplets had decayed and $P680^+$ was re-reduced. Knowing the actual high F_m/F_o ratio, the peak denoted F_m in Steffen et al. (2005) was significantly underestimated—most likely because TyrZ was simultaneously oxidized but not considered as a quencher.

The partial quenching of excitation to the level $F_f < F_m$ by oxidized TyrZ is difficult to explain. Earlier (Laisk et al. 2012), we suggested a photochemical quenching hypothesis, based on cycling of electrons within PSII bypassing Q_A. Since tyrosine is to some extent similar to quinone functioning as an electron carrier, Laisk et al. (2012) and Laisk and Oja (2013) suggested electron cycling in a triangular pathway.

$$TyrZ_{ox}P680 + h\nu \rightarrow TyrZ_{ox}P680 * \rightarrow TyrZP680^+ \rightarrow TyrZ_{ox}P680$$

In the state of oxidized TyrZ and reduced P680 and Q_A, the excited electron leaves P680* quenching excitation, but arrives at $TyrZ_{ox}$, from where it rapidly cycles to oxidized

P680. This cycle would need only 1 µs of electron transfer time from TyrZ to $P680^+$, plus about 2 ns for electron transfer from excited P680* to $TyrZ_{ox}$. Such a fast charge transfer from the excited Chl_{D1} to oxidized TyrZ would be allowed by the tunneling distance of about 8 Å between these electron carriers (Umena et al. 2011), but the problem is the too large free energy gap (Moser et al. 2005). During laser flashes of many excitations per µs, this model would still predict the accumulation of $P680^+$ with reduced TyrZ, which would quench fluorescence below F_o right after the flash—as actually reported by Belyaeva et al. (2015), but suggested to be the quenching by ^{3}Car. Although not conclusive, these arguments still allow oxidized TyrZ to quench excitation non-photochemically.

The obvious discrepancy between the fluorescence-based and O_2-based electron transport (Oja et al. 2011; Laisk et al. 2012; Laisk and Oja 2013) increased with light intensity, suggesting a mechanism similar to the Geiger–Müller counter of nuclear particles: after every photon transporting an electron, a dead time follows, during which photons absorbed by the antenna are lost for charge transfer (Laisk and Oja 2013). Due to the assumed possibility of double oxidation (accumulation of $TyrZ_{ox}$ and $P680^+$) generating a strong quencher, the discrepancy—expressed as the dead time τ after each successful electron transfer—is low (dead time short) at low PFDs and increases non-linearly with rising PFD. This is caused by the buffering effect of the double oxidation: in the single oxidation case, the second photon is lost in pairs separated by time interval $< \tau$, but in the double oxidation case only the third photon is lost in triples separated by time interval $< \tau$. In the single oxidation case, the dead time is constant, but in the double oxidation case the effective dead time is shorter than that of the single oxidation case at low light intensities, approaching the single oxidation value with increasing light intensity (Fig. 11b). The measured dependence of the type of Fig. 11a was not concave as predicted by the double oxidation, but rather was convex, transforming into decreasing τ with increasing light intensity (Laisk and Oja 2013). This experiment however was not definite due to the limited amplitude of PSII excitation rate. More significant may be the very low 810-nm signal from $P680^+$ detected in sunflower leaves at a PFD of 7000 µmol m^{-2} s^{-1}, equivalent to 2% of the full signal from $P700^+$ (Laisk et al. 2012). At this PFD, the Y_oP_o forms were calculated to accumulate up to 20% of all PSII forms (Fig. 4d). Experimentally, $P680^+$ has been detected only when the water-splitting complex was inhibited (Steffen et al. 2005; Belyaeva et al. 2014, 2015). Thus, it may be possible that the state with TyrZ oxidized but P680 unoxidized is unable for photochemical charge transfer.

In conclusion, the post-flash fluorescence yield F_f is observed when TyrZ is oxidized. Therefore, we *relate* the quenching to TyrZ, but cannot say that oxidized TyrZ is the quencher. Our model explains the S-state-dependent *rate* of relaxation of the F_f quenching, but not the S-state dependency of the F_f *level*. These facts still leave room for transmembrane electric field and proton concentration, as well as for protein conformational changes as factors controlling excitation quenching.

Acknowledgements This work was supported by Personal Grant No. 393P from Estonian Ministry of Education and Science and by personal support to A.L. from Estonian Academy of Science. Comments and help by R. Peterson (Scientist Emeritus, The Connecticut Agricultural Experiment Station) are highly appreciated.

References

Baake E, Schlöder JP (1992) Modeling the fast fluorescence rise of photosynthesis. Bull Math Biol 54:999–1021

Baake E, Strasser RJ (1990) A differential equation model for the description of the fast fluorescence rise (O-I-D-P-transient) in leaves. In: Current research in photosynthesis vol.I. Kluwer, The Netherlands

Belyaeva NE, Pashchenko VZ, Renger G, Riznichenko GY, Rubin AB (2006) Application of a photosystem II model for analysis of fluorescence induction curves in the 100 ns to 10 s time domain after excitation with a saturating light pulse. Biophysics 51:860–872

Belyaeva NE, Bulychev AA, Riznichenko GY, Rubin AB (2011) A model of photosystem II for the analysis of fast fluorescence rise in plant leaves. Biophysics Pleiades Publ 56:464–477

Belyaeva NE, Schmitt F-J, Paschenko VZ, Riznichenko GY, Rubin AB, Renger G (2014) Model based analysis of transient fluorescence yield induced by actinic laser flashes in spinach leaves and cells of green alga *Chlorella pyrenoidosa* Chick. Plant Physiol Biochem 77:49–59

Belyaeva NE, Schmitt F-J, Paschenko VZ, Riznichenko GY, Rubin AB (2015) Modeling of the redox state dynamics in photosystem II of *Chlorella pyrenoidosa* Chick cells and leaves of spinach and Arabidopsis thaliana from single flash-induced fluorescence quantum yield changes on the 100 ns–10 s time scale. Photosynth Res 125:123–140

Bowes JM, Crofts AR (1980) Binary oscillations in the rate of oxidation of the primary acceptor of Photosystem II. Biochim Biophys Acta 590:373–384

Christen G, Reifarth F, Renger G (1998) On the origin of the '35-µs kinetics' of $P680^{+\cdot}$ reduction in photosystem II with an intact water oxidizing complex. FEBS Lett 429:49–52

Crofts AR, Wraight CA (1983) The electrochemical domain of photosynthesis. Biochim Biophys Acta 726(2):149–185

de Wijn R, van Gorkom HJ (2001) Kinetics of electron transfer from Q_A to Q_B in photosystem II. BioChemistry 40:11912–11922

Delosme R (1967) Étude de l'induction de fluorescence des algues vertes et des chloroplastes an début d'une illumination intense. Biochim Biophys Acta 143:108–128

Duysens LNM, Sweers HE (1963) Mechanisms of two photochemical reactions in algae as studied by means of fluorescence. In: Physiologists JSoP (ed) Studies on microalgae and photosynthetic bacteria, special issue of plant and cell physiology. University of Tokyo Press, Tokyo, pp 353–372

Haferkamp S, Haase W, Pascal AA, van Amerongen H, Kirchhoff H (2010) Efficient light harvesting by photosystem II requires an

optimized protein packing density in grana thylakoids. J Biol Chem 285:17020–17028
Jablonsky J, Lazar D (2008) Evidence for intermediate S-states as initial phase in the process of oxygen-evolving complex oxidation. Biophysical J 94:2725–2736
Joliot A, Joliot P (1964) Étude cinétique de la réaction photochimique libérant l'oxygène au cours de la photosynthése. C R Acad Sc Paris 258:4622–4625
Joliot P, Joliot A (1977) Evidence for a double hit process in photosystem II based on fluorescence studies. Biochim Biophys Acta 462:559–574
Joliot P, Joliot A (1981) Double photoreactions induced by laser flash as measured by oxygen emission. Biochim Biophys Acta 638:132–140
Joliot P, Lavergne J, Béal D (1992) Plastoquinone compartmentation in chloroplasts. I. Evidence for domains with different rates of photo-reduction. Biochim Biophys Acta 1101:1–12
Kirchhoff H, Horstmann S, Weis E (2000) Control of the photosynthetic electron transport by PQ diffusion microdomains in thylakoids of higher plants. Biochim Biophys Acta 1459:148–168
Koblížek M, Kaftan D, Nedbal L (2001) On the relationship between the non-photochemical quenching of the chlorophyll fluorescence and the photosystem II light harvesting efficiency. A repetitive flash fluorescence induction study. Photosynth Res 68:141–152
Kolber Z, Prasil O, Falkowski PG (1998) Measurements of variable chlorophyll fluorescence using fast repetition rate technique. I. Defining methodology and experimental protocols. Biochim Biophys Acta 1367:88–106
Laisk A, Oja V (2013) Thermal phase and excitonic connectivity in fluorescence induction. Photosynth Res 117:431–448
Laisk A, Oja V, Eichelmann H (1994) Dependence between the quantum yield of photosystem II and chlorophyll fluorescence at constant nonphotochemical quenching. In: BBSRC Second Robert Hill symposium on photosynthesis. Imperial College of Science, Technology and Medicine, London, pp 59–60
Laisk A, Rasulov BH, Loreto F (1998) Thermoinhibition of photosynthesis as analyzed by gas exchange and chlorophyll fluorescence. Russian J Plant Physiol 45(4):412–421
Laisk A, Nedbal L, Govindjee (eds) (2009) Photosynthesis in silico. Understanding complexity from molecules to ecosystems. Advances in photosynthesis and respiration, vol 29. Springer, Dordrecht
Laisk A, Eichelmann H, Oja V (2012) Oxygen evolution and chlorophyll fluorescence from multiple turnover light pulses: charge recombination in photosystem II in sunflower leaves. Photosynth Res 113:145–155
Laisk A, Eichelmann H, Oja V (2015) Oxidation of plastohydroquinone by photosystem II and by dioxygen in leaves. Biochim Biophys Acta 1847:565–575
Laisk A, Oja V, Eichelmann H (2016) Kinetics of plastoquinol oxidation by the Q-cycle in leaves. Biochim Biophys Acta 1857:819–830
Lavergne J, Joliot P (1991) Restricted diffusion in photosynthetic membranes. TIBS 16:129–134
Lazár D (2003) Chlorophyll a fluorescence rise induced by high light illumination of dark-adapted plant tissue studied by means of a model of photosystem II and considering photosystem II heterogeneity. J Theor Biol 220:469–503
Lazár D (2009) Modelling of light-induced chlorophyll a fluorescence rise (O-J-I-P transient) and changes in 820 nm-transmittance signal of photosynthesis. Photosynthetica 47:483–498
Lazár D (2013) Simulations show that a small part of variable chlorophyll a fluorescence originates in photosystem I and contributes to overall fluorescence rise. J Theor Biol 335:249–264
Lazár D, Jablonsky J (2009) On the approaches applied in formulation of a kinetic model of photosystem II: different approaches lead to different simulations of the chlorophyll a fluorescence transients. J Theor Biol 257:260–269
Lazár D, Schansker G (2009) Models of chlorophyll a fluorescence transients. In: Laisk A, Nedbal L, Govindjee (eds) Photosynthesis in silico. Understanding complexity from molecules to ecosystems. Springer Science + Business Media B.V., Dordrecht, pp 85–123
Lebedeva GV, Belyaeva NE, Demin OV, Riznichenko GY, Rubin AB (2002) Kinetic model of primary photosynthetic processes in chloroplasts. Description of the fast phase of chlorophyll fluorescence induction under different light intensities. Biophysics 47(966):968–980 Translated from Russian Biofizika, Vol. 947, No. 966, 2002, pp. 1044–1058
Moser CC, Page CC, Dutton PL (2005) Tunneling in PSII. Photochem Photobiol Sci 4:933–939
Neubauer C, Schreiber U (1987) The polyphasic rise of chlorophyll fluorescence upon onset of strong continuous illumination: I. Saturation characteristics and partial control by the photosystem II acceptor side. Z Naturforschung 42c:123–131
Novoderezhkin VI, Romero E, van Grondelle R (2015) How exciton-vibrational coherences control charge separation in the photosystem II reaction center. Phys Chem Chem Phys 17:30828–30841
Oja V, Eichelmann H, Anijalg A, Rämma H, Laisk A (2010) Equilibrium or disequilibrium? A dual-wavelength investigation of photosystem I donors. Photosynth Res 103:153–166
Oja V, Eichelmann H, Laisk A (2011) Oxygen evolution from single- and multiple-turnover light pulses: temporal kinetics of electron transport through PSII in sunflower leaves. Photosynth Res 110:99–109
Osmond B, Chow WS, Wyber R, Zavafer A, Keller B, Pogson BJ, Robinson SA (2017) Relative functional and optical absorption cross-sections of PSII and other photosynthetic parameters monitored in situ, at a distance with a time resolution of a few seconds, using a prototype light induced fluorescence transient (LIFT) device. Functional Plant Biol. doi:10.1071/FP17024
Paillotin G, Geactinov NE, Breton J (1983) A master equation theory of fluorescence induction, photochemical yield, and singlet-triplet exciton quenching in photosynthetic systems. Biophys J 44:65–77
Peterson RB, Oja V, Eichelmann H, Bichele I, Dall'Osto L, Laisk A (2014) Fluorescence F_0 of photosystems II and I in developing C_3 and C_4 leaves, and implications on regulation of excitation balance. Photosynth Res 122:41–56
Rappaport F, Blanchard-Desce M, Lavergne J (1994) Kinetics of electron transfer and electrochromic change during the redox transitions of the photosynthetic oxygen-evolving complex. Biochom Biophys Acta 1184:178–192
Renger G (2010) The light reactions of photosynthesis. Current Sci 98:1305–1319
Robinson H, Crofts AR (1983) Kinetics of the oxidation-reduction reactions of the photosystem II quinone acceptor complex, and the pathway for deactivation. FEBS Lett 153:221–226
Samson G, Bruce D (1996) Origin of the low yield of chlorophyll fluorescence induced by single turnover flash in spinach thylakoids. Biochim Biophys Acta 1276:147–153
Schansker G, To'th S, Kova'cs L, Holzwarth AR, Garab G (2011) Evidence for a fluorescence yield change driven by a light-induced conformational change within photosystem II during the fast chlorophyll a fluorescence rise. Biochim Biophys Acta 1807:1032–1043
Schansker G, Tóth SC, Holzwarth AR, Garab G (2014) Chlorophyll a fluorescence: beyond the limits of the Q_A model. Photosynth Res 120:43–58
Schreiber U (2002) Assessment of maximal fluorescence yield. Donor-side dependent quenching and Q_B-quenching. In: Van Kooten

O, Snel J (ed) Plant spectrophotometry: applications and basic research. Rozenberg, Amsterdam, pp 23–47

Schreiber U, Neubauer C (1987) The polyphasic rise of chlorophyll fluorescence upon onset of strong continuous illumination: II. Partial control by the photosystem II donor side and possible ways of interpretation. Z Naturforsch 42c:132–141

Schreiber U, Klughammer C, Kolbowski J (2012) Assessment of wavelength-dependent parameters of photosynthetic electron transport with a new type of multi-color PAM chlorophyll fluorometer. Photosynth Res 113:127–144

Shinkarev VP (2004) Photosystem II: oxygen evolution and chlorophyll a fluorescence induced by multiple flashes. In: Papageorgiou GC, Govindjee (eds) Chlorophyll a fluorescence: a signature of photosynthesis. Springer, Dordrecht, pp 197–229

Steffen R, Eckert H-J, Kelly AA, Dörmann PG, Renger G (2005) Investigations on the reaction pattern of photosystem II in leaves from *Arabidopsis thaliana* by time-resolved fluorometric analysis. BioChemistry 44:3123–3132

Stirbet A, Govindjee (2012) Chlorophyll a fluorescence induction: a personal perspective of the thermal phase, the J-I-P rise. Photosynth Res 113:15–61

Strasser BJ (1997) Donor side capacity of photosystem II probed by chlorophyll *a* fluorescence transients. Photosynth Res 52:147–155

Strasser RJ, Govindjee (1991) The F_0 and the O-J–I–P fluorescence rise in higher plants and algae. In: A-A JH (ed) Regulation of chloroplast biogenesis. Plenum Press, New York, pp 423–426

Strasser R, Tsimili-Michael M, Srivastava A (2004) Analysis of the chlorophyll a fluorescence transient. In: Papageorgiou GC, Govindjee (eds) Chlorophyll a fluorescence. A signature of photosynthesis. Springer, Dordrecht, pp 321–362

Sušila P, Lazár D, Ilik P, Tomek P, Nauš P (2004) The gradient of exciting radiation within a sample affects the relative height of steps in the fast chlorophyll *a* fluorescence rise. Photosynthetica 42:161–172

Tóth SZ, Schansker G, Strasser RJ (2005a) In intact leaves, the maximum fluorescence level (F_M) is independent of the redox state of the plastoquinone pool: a DCMU-inhibition study. Biochim Biophys Acta 1708:275–282

Tóth SZ, Schansker G, Strasser RJ (2005b) In intact leaves, the maximum fluorescence level (FM) is independent of the redox state of the plastoquinone pool: a DCMU-inhibition study. Biochim Biophys Acta 1708:275–282

Tóth SZ, Schansker G, Garab G, Strasser RJ (2007a) Photosynthetic electron transport activity in heat-treated barley leaves: the role of internal alternative electron donors to photosystem II. Biochim Biophys Acta 1767:295–305

Tóth SZ, Schansker G, Strasser RJ (2007b) A non-invasive assay of the plastoquinone pool redox state based on the OJIP-transient. Photosynth Res 93:193–203

Umena Y, Kawakami K, Shen J-R, Kamiya N (2011) Crystal structure of oxygen-evolving photosystem II at a resolution of 1.9 Å. Nature 473:55–61

Vredenberg VJ (2008a) Algorithm for analysis of OJDIP fluorescence induction curves in terms of photo- and electrochemical events in photosystems of plant cells. Derivation and application. J Photochem Photobiol B 91:58–65

Vredenberg WJ (2008b) Analysis of initial chlorophyll fluorescence induction kinetics in chloroplasts in terms of rate constants of donor side quenching release and electron trapping in photosystem II. Photosynth Res 96:83–97

Vredenberg W (2015) A simple routine for quantitative analysis of light and dark kinetics of photochemical and non-photochemical quenching of chlorophyll fluorescence in intact leaves. Photosynth Res 124:87–106

Vredenberg W, Durchan M, Prášil O (2007) On the chlorophyll a fluorescence yield in chloroplasts upon excitation with twin turnover flashes (TTF) and high frequency flash trains. Photosynth Res 93:183–192

Vredenberg W, Durchan M, Prášil O (2009) Photochemical and photoelectrochemical quenching of chlorophyll fluorescence in photosystem II. Biochim Biophys Acta 1787:1468–1478

Xu Q, Baciou L, Sebban P, Gunner MR (2002) Exploring the energy landscape for Q_A^- to Q_B electron transfer in bacterial photosynthetic reaction centers: effect of substrate position and tail length on the conformational gating step. BioChemistry 41:10021–10025

Zhu X-G, Govindjee, Baker NR, deSturler E, Ort DR, Long SP (2005) Chlorophyll a fluorescence induction kinetics in leaves predicted from a model describing each discrete step of excitation energy and electron transfer associated with photosystem II. Planta 223:114–133